Trace Element and Sulfur Isotope Signatures of Volcanogenic Massive Sulfide (VMS) Mineralization: A Case Study from the Sunnhordland Area in SW Norway

Sabina Strmic Palinkas [1,2,*], **Trond Fjellet** [2], **Håvard Hallås Stubseid** [2], **Xuan Liu** [3], **Jorge Enrique Spangenberg** [4], **Andrea Čobić** [5] **and Rolf Birger Pedersen** [2]

1 Department of Geosciences, Faculty of Sciences and Technology, UiT The Arctic University of Norway, Dramsvegen 201, N-9037 Tromsø, Norway

2 Centre for Deep Sea Research, Department of Earth Science, Faculty of Mathematics and Natural Sciences, University of Bergen, Allegaten 41, N-5007 Bergen, Norway; trfjellet@gmail.com (T.F.); havard.stubseid@uib.no (H.H.S.); rolf.pedersen@uib.no (R.B.P.)

3 Geological Survey of Finland, P.O. Box 96, FI-02151 Espoo, Finland; xuan.liu@gtk.fi

4 Institute of Earth Surface Dynamics, University of Lausanne, Geopolis, CH-1015 Lausanne, Switzerland; jorge.spangenberg@unil.ch

5 Department of Geology, Faculty of Science, University of Zagreb, Horvatovac 95, HR-10000 Zagreb, Croatia; andrea.cobic@geol.pmf.unizg.hr

* Correspondence: sabina.s.palinkas@uit.no

Abstract: The Sunnhordland area in SW Norway hosts more than 100 known mineral occurrences, mostly of volcanogenic massive sulfide (VMS) and orogeny Au types. The VMS mineralization is hosted by plutonic, volcanic and sedimentary lithologies of the Lower Ordovician ophiolitic complexes. This study presents new trace element and $\delta^{34}S$ data from VMS deposits hosted by gabbro and basalt of the Lykling Ophiolite Complex and organic-rich sediments of the Langevåg Group. The Alsvågen gabbro-hosted VMS mineralization exhibits a significant Cu content (1.2 to >10 wt.%), with chalcopyrite and cubanite being the main Cu-bearing minerals. The enrichment of pyrite in Co, Se, and Te and the high Se/As and Se/Tl ratios indicate elevated formation temperatures, while the high Se/S ratio indicates a contribution of magmatic volatiles. The $\delta^{34}S$ values of the sulfide phases also support a substantial influx of magmatic sulfur. Chalcopyrite from the Alsvågen VMS mineralization shows significant enrichment in Se, Ag, Zn, Cd and In, while pyrrhotite concentrates Ni and Co. The Lindøya basalt-hosted VMS mineralization consists mainly of pyrite and pyrrhotite. Pyrite is enriched in As, Mn, Pb, Sb, V, and Tl. The $\delta^{34}S$ values of sulfides and the Se/S ratio in pyrite suggest that sulfur was predominantly sourced from the host basalt. The Litlabø sediment-hosted VMS mineralization is also dominated by pyrite and pyrrhotite. Pyrite is enriched in As, Mn, Pb, Sb, V and Tl. The $\delta^{34}S$ values, which range from −19.7 to −15.7 ‰ VCDT, point to the bacterial reduction of marine sulfate as the main source of sulfur. Trace element characteristics of pyrite, especially the Tl, Sb, Se, As, Co and Ni concentrations, together with their mutual ratios, provide a solid basis for distinguishing gabbro-hosted VMS mineralization from basalt- and sediment-hosted types of VMS mineralization in the study area. The distinctive trace element features of pyrite, in conjunction with its sulfur isotope signature, have been identified as a robust tool for the discrimination of gabbro-, basalt- and sediment-hosted VMS mineralization.

Keywords: volcanogenic massive sulfide (VMS) deposits; pyrite; trace element geochemistry; sulfur isotope ($\delta^{34}S$) systematics; the Upper Allochthone of the Scandinavian Caledonides

1. Introduction

Volcanogenic massive sulfide (VMS) deposits have traditionally been mined for Cu, Zn and eventually Pb, with Au and Ag as common by-products. Recently, this type of

mineralization has gained attention due to its potential enrichment in numerous technology-critical elements such as Co, Ni, Mn, Cd, In, Sn, Se, Bi, Te, Ga, Ge and Sb (e.g., [1–3]). The VMS deposits represent a product of convective hydrothermal circulation within the seafloor, driven by a combination of extensional tectonics and an elevated geothermal gradient (e.g., [4]). This type of mineralization has been found in various ancient and recent geological settings, including mid-ocean ridges, back-arc basins, intra-oceanic arc systems and continental arc rifts (e.g., [5–7]). The mineralization is dominated by pyrite and pyrrhotite and has a stratiform character. Depending on its geological setting, VMS mineralization can be hosted by hydrothermally altered ultramafic, mafic or felsic magmatic rocks or by siliciclastic sedimentary sequences (e.g., [5,8,9]).

Mining of VMS deposits in Norway has a tradition of over 450 years. During this time, more than 100 Mt of ore have been mined in 10 major mining districts located along the Upper Allochthon of the Scandinavian Caledonides, an orogenic belt that extends for about 1500 km from the Stavanger region in southern Norway to the Barents Sea region in northern Norway (e.g., [10,11]; Figure 1). The VMSVMS mineralization is predominantly associated with two generations of ophiolite terranes of the Iapetus Ocean realm. The Early Ordovician ophiolites exhibit a range of compositions from MORB, IAT, boninites and calc-alkaline to alkaline basalts, whereas the Late Ordovician ophiolite complexes are characterized by N- to E-MORB compositions [11–13].
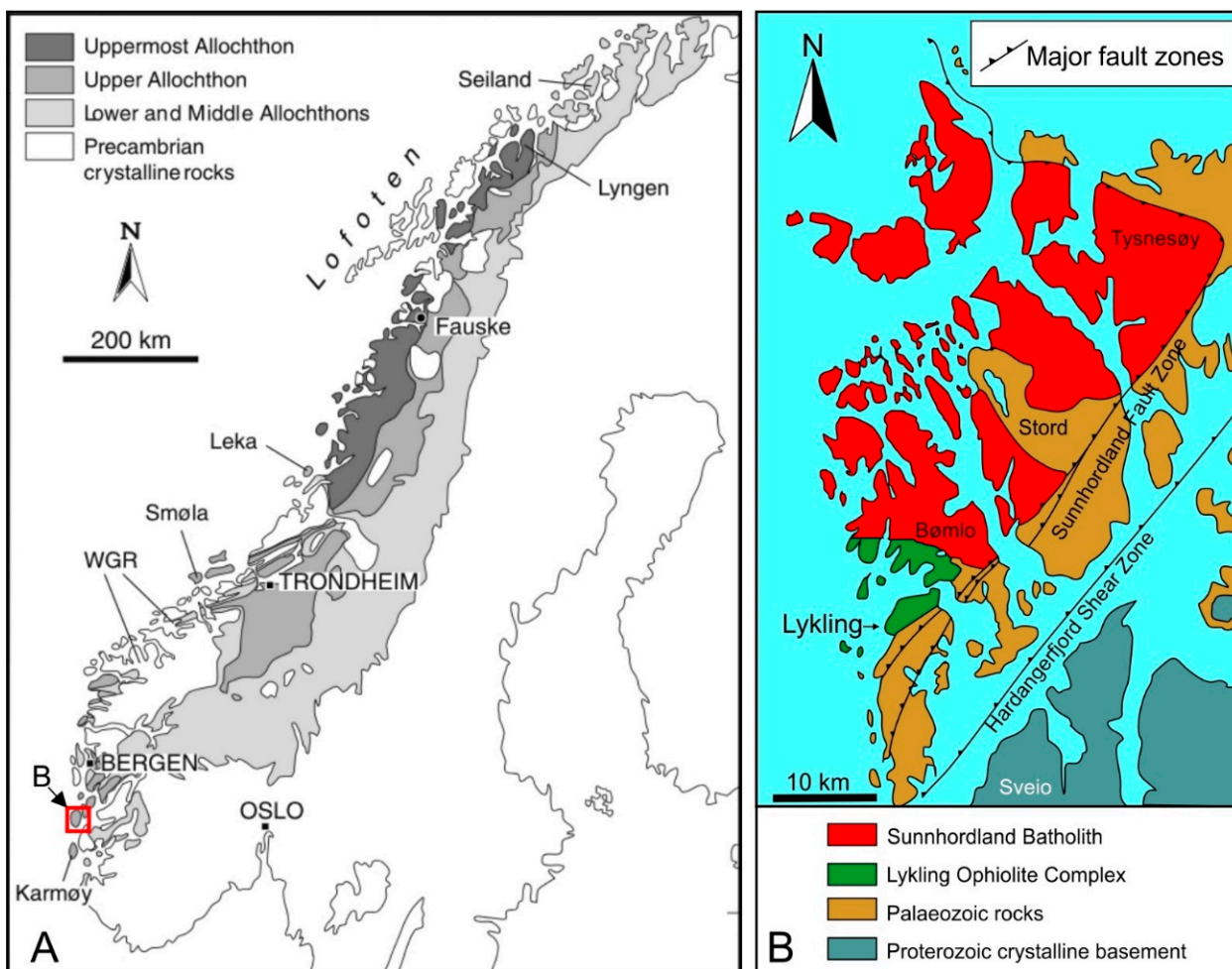
Figure 1. (**A**) Simplified geological map of the Scandinavian Caledonides (after [14]) showing the location of the most prominent ophiolite complexes and the study area marked by a red square; (**B**) Geological setting of the Sunnhordland region in the Upper Allotone of the Scandinavian Caledonides (after [10]).

The Sunnhordland area in SW Norway hosts more than 100 known mineral occurrences, most of them of the VMS and orogeny Au types (Figure 2; [10,15,16]). The VMS mineralization in this area is associated with the Early Ordovician ophiolitic terranes. Depending on their immediate host rock, the deposits can be categorized into three main groups: (1) gabbro-hosted VMS deposits, (2) basalt-hosted VMS deposits, and (3) sediment-hosted VMS deposits. Despite the abundance and diversity of the VMS occurrences in the Sunnhordland region, their mineralogical and geochemical characteristics, as well as the genetic models, have been poorly constrained [10].

This paper presents new data on ore mineralogy, multi-element LA-ICP-MS analyses and sulfur isotope (δ^{34}S) obtained from gabbro-, basalt- and sediment-hosted VMS deposits in the Sunnhordland area, SW Norway (Figure 1). The main objective of the study is to reveal the trace element and stable isotope characteristics of sulfide minerals associated with VMS mineralization hosted by diverse lithologies and thus contribute to the advancement of geochemical exploration methodology.

2. Geological Setting

2.1. Regional Geology

Scandinavian Caledonides (Figure 1), an orogenic belt underlaid by the Fennoscandian shield, document an approximately 900 Ma year-long geological history that began with the breakup of Rodinia [17], which was followed by the opening of the Iapetus Ocean (e.g., [10,11,18]). The closure of the Iapetus Ocean in the Late Cambrian cumulated with the subduction of the Baltica terrains beneath Laurentia in the late Silurian to Early Devonian. During an oblique collision episode, the allochthonous tectonic units were accreted onto the Baltic continent [14,19,20]. The Devonian period is characterized by post-collisional processes associated with extensional tectonics, the formation of basins and extensive sedimentation [14].

The Sunnhordland region is composed of Precambrian basement rocks overlain by the Caledonian allochthonous units. The contact between the basement and the Caledonian lithologies is marked by the low-angle Hardangerfjord Shear Zone [21]. The VMS deposits are exclusively hosted within the Upper Allochthon ([10]; Figure 1), a tectono-stratigraphic unit composed of ophiolites, igneous and island arc complexes and several adjacent sedimentary basins (Figure 2). Based on their age and genetic features, the ophiolite complexes of the Upper Allochthon were divided into two generations: (1) Early Ordovician ophiolites (i.e., the Leka, Løkken, Gullfjellet, Lykling and Karmøy ophiolite complexes, as shown in Figure 2) that formed in an intra-oceanic arc environment, and (2) Late Ordovician ophiolites (i.e., the Solund-Stavfjord and Sulitjelma ophiolite complexes, as shown in Figure 2) that developed in a back-arc setting before the Laurentia-Baltica collision event [22–25].
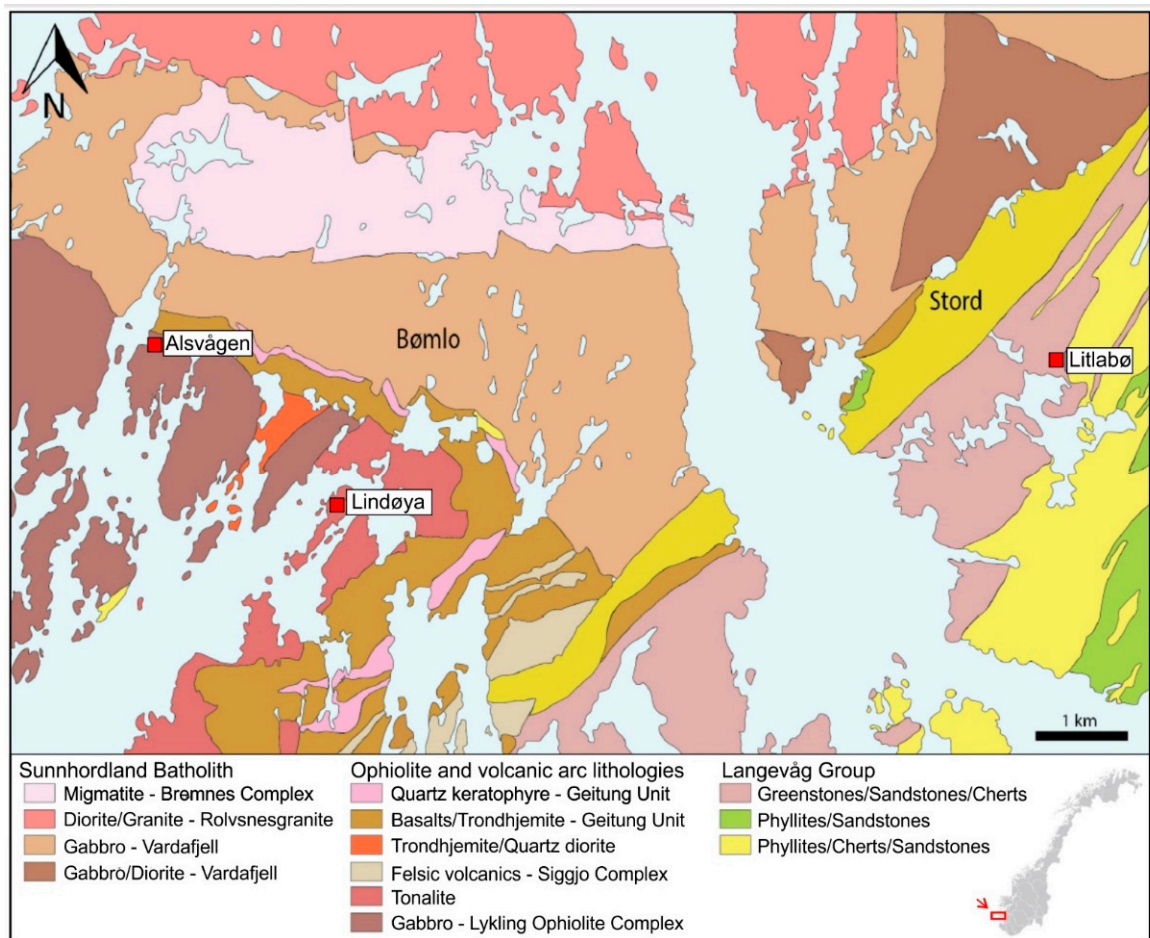
Figure 2. Geological map of the Sunnhordland region showing the locations of the investigated VMS deposits (Alsvågen gabbro-hosted VMS mineralization, Lindøya basalt-hosted VMS mineralization and Litlabø sediment-hosted VMS mineralization). The map is based on the 1:250,000 geological map of the Norwegian Geological Survey [26].

2.2. Geology of the Study Area

Stratigraphically, the lowermost part of the Bømlo island consists of the Lykling Ophiolite Complex, which is unconformably overlain by immature island arc lithologies of the Geitung Unit (Figure 2; [27]). The Lykling Ophiolite Complex records almost complete oceanic crust succession, including chromite-bearing serpentinites in its deepest part, overlain by layered and isotropic gabbro sequences, sheeted dyke complexes and basaltic pillow lavas [22,27,28]. The geochemical characteristics of its mafic lithologies suggest that the Lykling Ophiolite Complex was formed in a supra-subduction zone [29]. The Geitung Unit is made of dacites, basaltic pillow lavas, hyaloclastites and interbedded sediments [27]. Both the Lykling Ophiolite Complex and the overlying Geitung Unit were intruded by tonalite, trondhjemite and dacitic dykes [28].

The Langevåg Group is exposed along the southern parts of the islands of Bømlo and Stord (Figure 2). This volcano–sedimentary complex consists of six formations with a total thickness of ~1250 m, reflecting the progressive deepening of a marine back-arc basin [28]. The lowermost Krekjebær Formation records subaerial mafic volcanic activity. It is overlain by radiolarian cherts, turbidites, tuffs and possible submarine pyroclastic flows of the Kyrkjetuft Formation. The Vorland Formation and Stavaneset Formation mostly consist of green phyllites and sandstones sporadically intercalated with vesicular greenstones and radiolarian cherts [27,28]. These two units are stratigraphically separated with an over 100 m thick chert-bearing Hesthaugen Formation. The uppermost portion of the Langevåg

Group is represented by the Vespestad Formation, which mainly consists of dark shales and quartz-rich turbidites [28].

The Siggjo Complex unconformably overlies the Lykling Ophiolite Complex and the Geitung Unit (Figure 2; [27]). It predominantly consists of basalts and basaltic andesites with a calc-alkaline character [28]. The U/Pb dating of the andesites yielded 473 ± 2 Ma [29].

The northern parts of the islands of Bømlo and Stord are intruded by the Sunnhordland Batholith, an intrusive magmatic body with an area of about 1.000 km^2 (Figure 2; [30]). The batholith is composed of a range of mafic to felsic lithologies, including gabbros, diorites, granodiorites and granites. U/Pb dating of zircons indicates the gabbro emplacement at 472 ± 2 Ma [29], while the granites have been dated at 468 ± 3 Ma [31].

2.3. The VMS Mineralization in the Study Area

The Sunnhordland area in SW Norway hosts more than 100 known mineral occurrences, including VMS deposits hosted by plutonic and volcanic lithologies as well as sediments (e.g., [10,15]). The Alsvågen and Lindøya VMS deposits are the largest known VMS occurrences associated with the Lykling Ophiolite Complex (Figure 2). The Alsvågen mineralization is hosted by the gabbroic sequence, while the Lindøya mineralization is hosted by overlying basalts. The Litlabø VMS deposit, on the other hand, is hosted by sedimentary rocks of the Langevåg Group. With over 9 Mt of ore historically mined, Litlabø is known as the largest VMS deposit in the entire Sunnhordland region (Figure 2).

The southern part of the Alsvågen area is dominated by barren layered and isotropic gabbro of the Lykling Ophiolite Complex. Mineralization occurs in the northern part of the Alsvågen area, where the layered gabbro becomes scarcer and is replaced by altering coarse- and micro-gabbroic lithologies. The contact between the coarse- and micro-gabbro is often sharp, indicating a high-level gabbroic zone where micro-gabbroic dykes have intruded coarser-grained isotropic gabbro. A younger generation of east–west orientated basaltic dykes crosscut the Alsvågen area. The entire area was affected by the greenschist facies regional metamorphism during the Caledonian orogeny [32,33]. The Alsvågen region contains four mineralized shear zones trending NW–SE (Figure 3A). While two of these shear zones are partially visible at the surface (Figure 4A), historical mining activities have removed a significant part of the mineralization they host. Mineralization along the shear zones has a massive appearance, mainly characterized by chalcopyrite and pyrrhotite as the predominant sulfide minerals. Away from the shear zones, the sulfide mineralization takes the form of disseminations and veinlets hosted by both coarse- and micro-gabbroic lithologies (Figure 4B; [33]).

The Lindøya area consists mainly of trondhjemite that has intruded into the Geitung Unit and the Lykling Ophiolite Complex (Figure 3). Micro-gabbro and basalt are exposed along the central part of the area, but their extent is still unknown. Younger basaltic dykes crosscut trondhjemite and possibly the micro-gabbro/basaltic lithologies. The main ore body is hosted by basalts. The mineralization, consisting predominantly of pyrite and minor amounts of chalcopyrite, occurs in the form of massive lenses and disseminations (Figure 4C; [33]).

The Litlabø mineralization is hosted by the volcano–sedimentary complex of the Langevåg Group (Figure 3), which documents the deepening of the back-arc basin [28]. The mineralization is embedded in organic-rich black shales (Figure 4D,E). It mostly occurs in the form of bedding-parallel massive sulfide layers predominantly composed of pyrite and pyrrhotite. Locally, pyrite-rich veinlets that crosscut the primary bedding were found (Figure 4F; [33]).
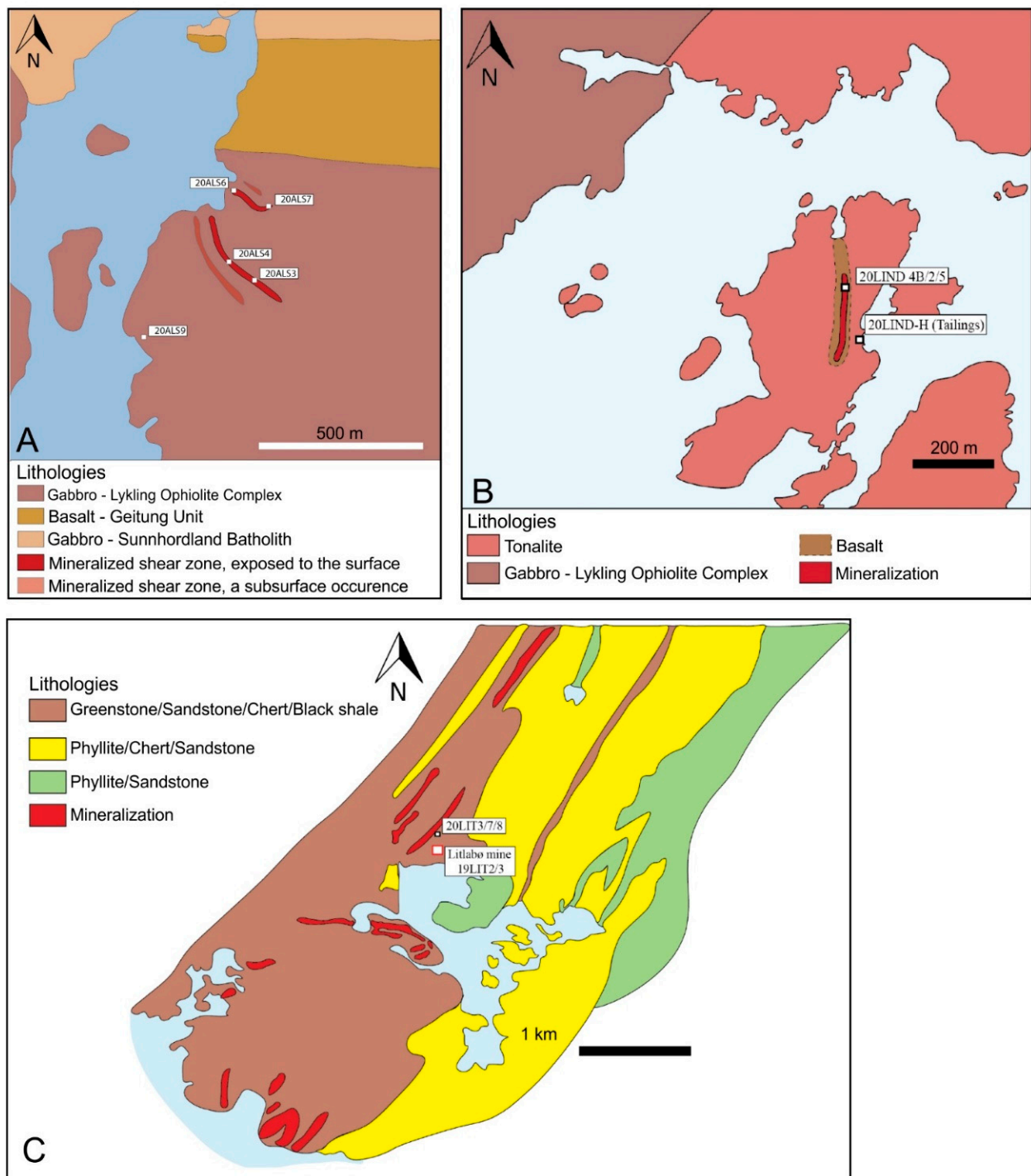
Figure 3. Local geological relationships at the study areas with labeled sampling locations: (**A**) Gabbro-hosted VMS mineralization in the Alsvågen area; (**B**) Basalt-hosted VMS mineralization in the Lindøya area; (**C**) Sediment-hosted VMS mineralization in the Litlabø area. The maps are based on the 1:250,000 geological map of the Norwegian Geological Survey [26].
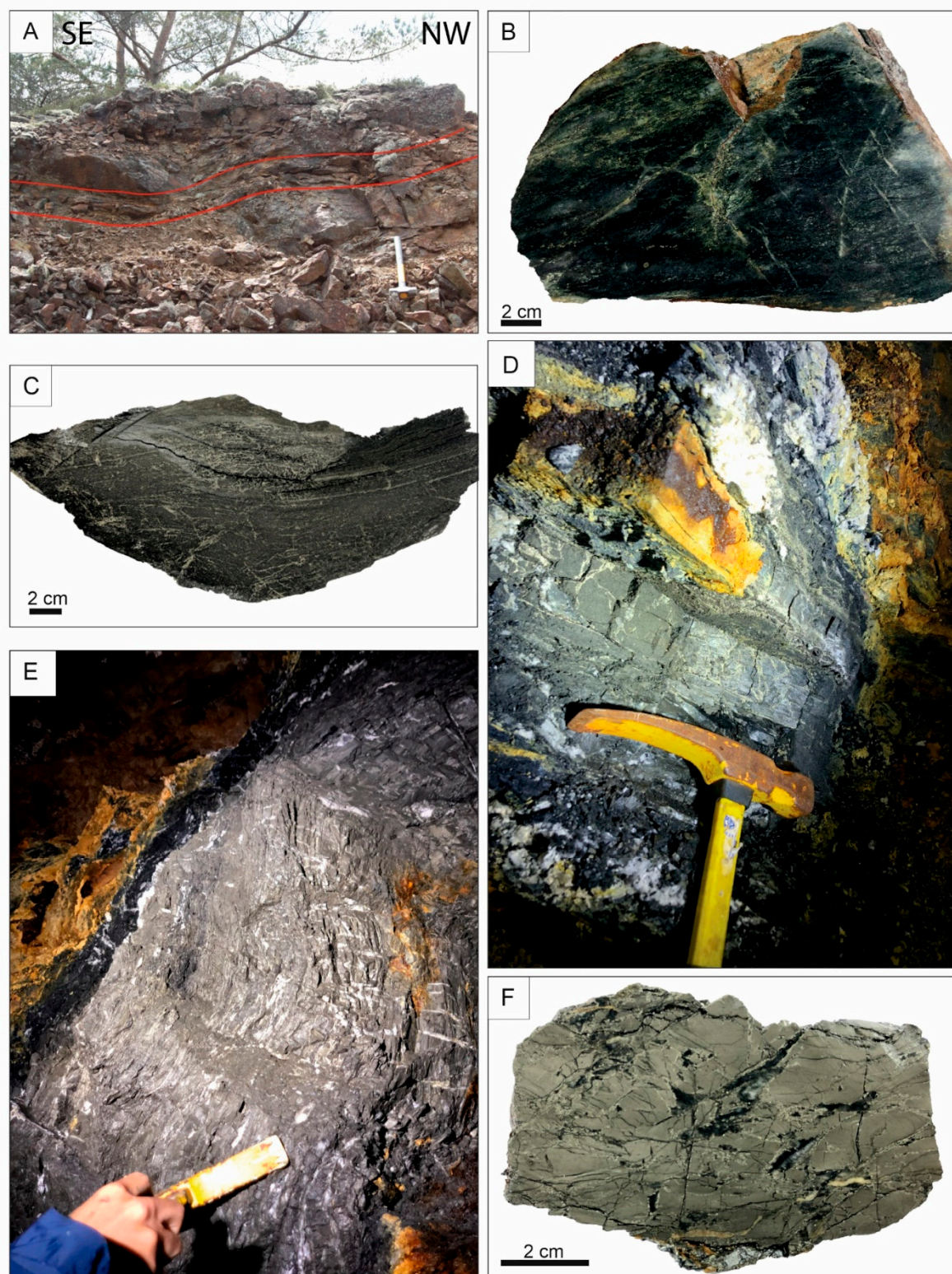
Figure 4. (**A**) Surface exposure of the northern shear zone in the Alsvågen gabbro-hosted deposit; (**B**) A hand specimen of weakly mineralized micro-gabbro from the Alsvågen gabbro-hosted deposit; (**C**) A hand specimen of the massive sulfide mineralization from the Lindøya basalt-hosted deposit; (**D**) Subsurface exposure of the bedding-parallel massive sulfide mineralization hosted by organic-rich shale in the Litlabø sediment-hosted deposit; (**E**) Subsurface exposure of the massive sulfide mineralization in the Litlabø sediment-hosted deposit; (**F**) A hand specimen of the massive sulfide mineralization from the Litlabø sediment-hosted deposit.

3. Samples and Methods

3.1. Samples

The sampling campaign in the Sunnhordland area (Figure 2) was carried out in the summer of 2020 as a part of TF's Master project. In total, over 40 samples of barren and mineralized host rocks and sulfide mineralization were collected, but the results presented in this paper are from 14 samples of sulfide mineralization (Figure 3). The representative samples were prepared as polished thick sections for petrography and in situ trace element analyses. The samples selected for ore grade analyses were pulverized in an agate mill. The mineral grains selected for sulfur isotope analyses were micro-drilled.

3.2. Analytical Methods

Petrographic studies were carried out on polished thick sections using reflected light microscopy. Textural features and semi-quantitative analyses of the mineralized samples were studied on carbon-coated polished sections using a Zeiss supra 55VP Scanning Electron Microscope (SEM) equipped with an Energy-Dispersive X-ray (EDX) spectrometer at the University of Bergen. EDX analyses were performed with a Thermo Noran detector at a working distance of 8.5 mm, an accelerating voltage of 20 kV and an aperture of 60 μm.

The ore grade was determined at Bureau Veritas Minerals, Canada. The multi-acid digestion and ICP-ES method (code MA370) was combined with the Fire Assay Au method (code FA330-Au). A total of 24 elements were analyzed. Their detection limits are listed in Table 1.

Laser ablation single collector ICP-MS analyses of sulfide minerals were performed at the Geological Survey of Finland (GTK), using a Nu AttoM SC-ICPMS (Nu Instruments Ltd., Wrexham, UK) and Excite193nm ArF laser-ablation system (Photon Machines, San Diego, USA). The laser was operated at a pulse frequency of 5 Hz and a pulse energy of 5 mJ at 40% attenuation with a spot size of 40 μm. Each analysis began with a 20 s baseline measurement followed by switching on the laser for 40 s for signal acquisition. Analyses were performed using time-resolved analysis (TRA) with continuous data acquisition for each set of points (generally following the scheme of primary standard, quality control standard, 10–15 unknowns). Measurements were performed at low resolution (M/ΔM = 300) in fast-scanning mode. The synthetic pressed nanopellet sulfide standard UQAC FeS-1 was used for external standardization, and the nanopellet sulfide standards FeS-5 and FeS-6 were used as quality controls. Data reduction was performed using GLITTER TM software [34], which allows for baseline subtraction, the integration of the signal over a selected time resolve area and quantification using known concentrations of the external and internal standards. The isotope ^{57}Fe was used as the internal standard, assuming a stoichiometric composition.

Sulfur isotope analyses were carried out at the University of Lausanne, Switzerland, using elemental analysis and isotope ratio mass spectrometry (EA/IRMS). The EA/IRMS system consisted of a Carlo Erba 1108 elemental analyzer coupled with a continuous helium flow interface to a Thermo Fisher Delta V isotope ratio mass spectrometer [35]. The samples were combusted at 1030 °C in a single oxidation–reduction quartz tube filled with oxidizing (tungsten trioxide) and reducing (elemental copper) agents. The measured values of sulfur isotopes are given in the δ-notation and relative to the Vienna Cañon Diablo Troilite (VCDT) standard. The laboratory assured that the reproducibility with replicate analysis with given standards (natural pyrite –6.72 ‰, synthetic mercury sulfide, +15.82 ‰, barium sulfate, +12.73 ‰ δ^{34}S; [35]) is better than 0.2‰.

Table 1. The ore grade analysis of selected mineralized samples from the Alsvågen, Lindøya and Litlabø VMS deposits, SW Norway.

	Method	FA330	MA370	MA370	MA370	MA370	MA370	MA370	MA370	MA370	MA370	MA370	MA370	MA370	MA370	MA370	MA370	MA370	MA370	MA370	MA370	MA370	MA370	MA370	MA370
	Element	Au	Ag	Mo	Cu	Pb	Zn	Ni	Co	Mn	Fe	As	Sr	Cd	Sb	Bi	Ca	P	Cr	Mg	Al	Na	K	W	S
Sample	Unit d.l. *	ppb 2	ppm 2	wt.% 0.001	0.001	0.02	0.01	0.001	0.001	0.01	0.01	0.02	0.01	0.001	0.01	0.01	0.01	0.01	0.001	0.01	0.01	0.01	0.01	0.01	0.05
The Alsvågen gabbro-hosted VMS deposit																									
20ALS7S1		40	3	<0.001	3339	<0.02	0.01	<0.001	0.004	0.09	9.04	<0.02	0.02	<0.001	<0.01	<0.01	2.18	0.18	<0.001	1.55	8.50	4.39	0.21	<0.01	2.90
20ALS7S3		85	12	<0.001	>10.000	<0.02	0.04	0.006	0.029	0.02	15.02	<0.02	<0.01	<0.001	<0.01	<0.01	1.00	0.04	<0.001	0.90	1.58	0.17	0.03	<0.01	10.18
20ALS6D1		70	5	<0.001	5427	<0.02	0.03	0.010	0.036	0.04	19.47	<0.02	<0.01	<0.001	<0.01	<0.01	0.71	0.01	0.001	1.37	2.13	0.69	0.02	<0.01	7.86
20ALS3S1		45	3	<0.001	1196	<0.02	0.03	0.005	0.011	0.02	9.63	<0.02	<0.01	<0.001	<0.01	<0.01	0.13	<0.01	0.012	0.38	0.57	0.11	0.02	<0.01	5.76
The Lindøya basalt-hosted VMS deposit																									
20LIND4B		67	<2	0.004	0.008	<0.02	0.02	0.003	<0.001	0.03	30.61	0.03	<0.01	<0.001	<0.01	<0.01	0.16	<0.01	0.001	0.60	1.14	0.13	0.30	<0.01	>30.00
20LINDH		14	<2	<0.001	0.006	<0.02	0.01	0.001	<0.001	0.09	7.28	<0.02	<0.01	<0.001	<0.01	<0.01	0.96	0.07	<0.001	3.04	9.12	4.83	0.11	<0.01	4.19
The Litlabø sediment-hosted VMS deposit																									
19LIT3		201	<2	0.002	0.056	0.07	0.12	0.021	0.005	0.15	51.84	0.04	<0.01	<0.001	<0.01	<0.01	0.15	0.07	<0.001	0.17	0.36	0.03	0.12	<0.01	24.87
19LIT2		39	2	<0.001	0.035	<0.02	0.04	0.006	<0.001	0.07	38.40	0.05	<0.01	<0.001	<0.01	<0.01	0.70	<0.01	<0.001	0.17	0.69	<0.01	0.23	<0.01	>30.00

* *d.l.*—detection limit.

4. Results

4.1. Petrography of Host Rock and Ore Mineralization

4.1.1. The Alsvågen Gabbro-Hosted VMS Mineralization

VMS mineralization at Alsvågen is hosted by the gabbro of the Lykling Ophiolite Complex (Figure 3A). Barren layered gabbro consists predominantly of amphiboles, saussurite and chlorites (Figure 5A,B), indicating a regional metamorphic overprint. The mineral composition of slightly mineralized isotropic gabbro is also characterized by abundant amphiboles and chlorites, whereas plagioclase shows only weak saussuritization (Figure 5C,D). Minor amounts of epidote were also observed (Figure 6A). The abundant occurrence of quartz indicates that the mineralization event was associated with extensive silicification. The gabbro in the immediate vicinity of the mineralized shear zones is composed of amphiboles, chlorites, weakly saussuritized plagioclase and quartz and locally records epidotization (Figure 5E,F).
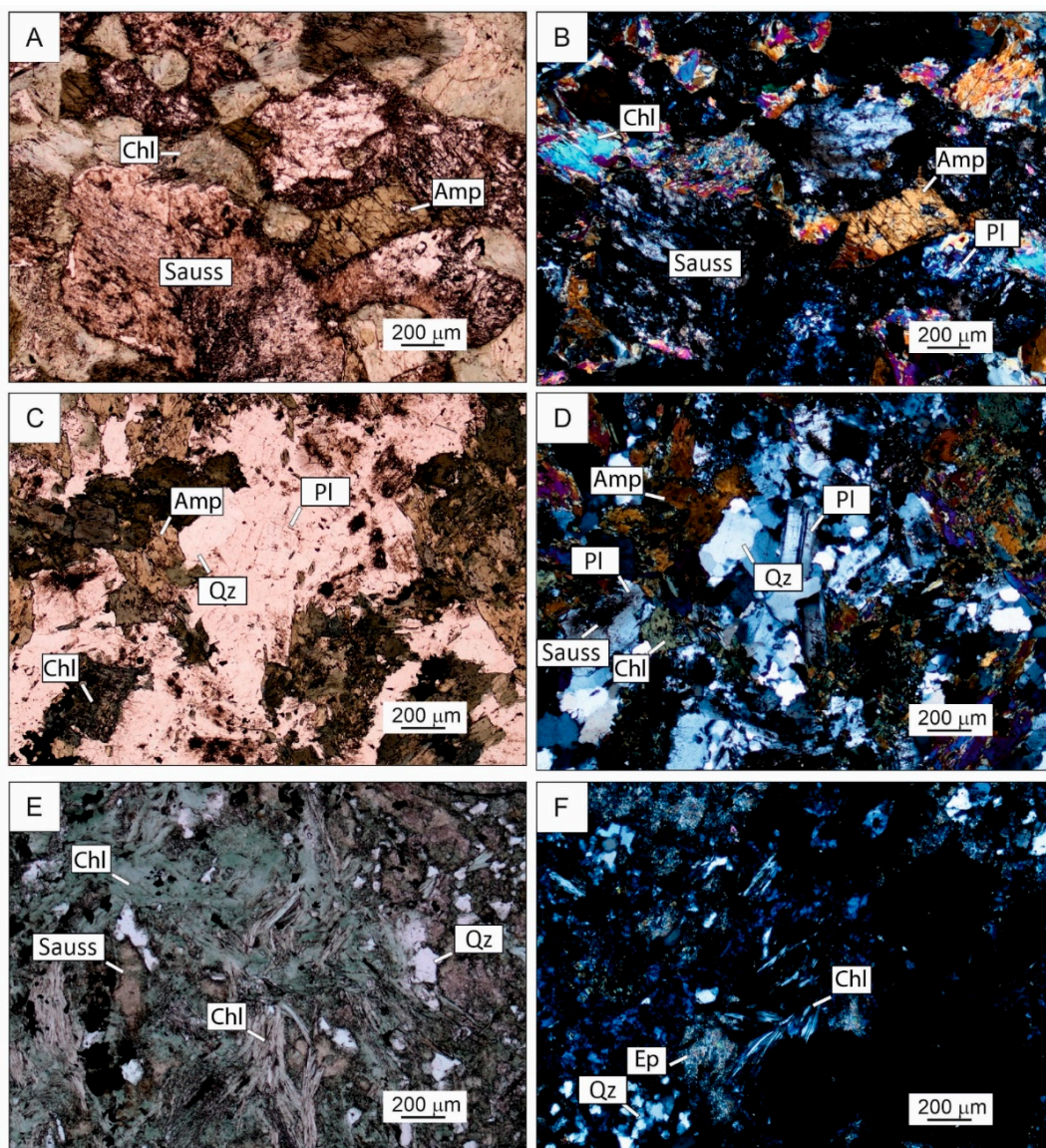
Figure 5. Microphotographs of: (**A**) Barren layered gabbro (PPL); (**B**) Barren layered gabbro (XPL); (**C**) Weakly mineralized isotropic gabbro (PPL); (**D**) Weakly mineralized isotropic gabbro (XPL); (**E**) Mineralized micro-gabbro from (PPL); (**F**) Mineralized micro-gabbro (XPL). Mineral abbreviations are according to [36]; Amp—amphibole, Chl—chlorite, Ep—epidote, Pl—plagioclase, Qz—quartz, Sauss—saussurite.
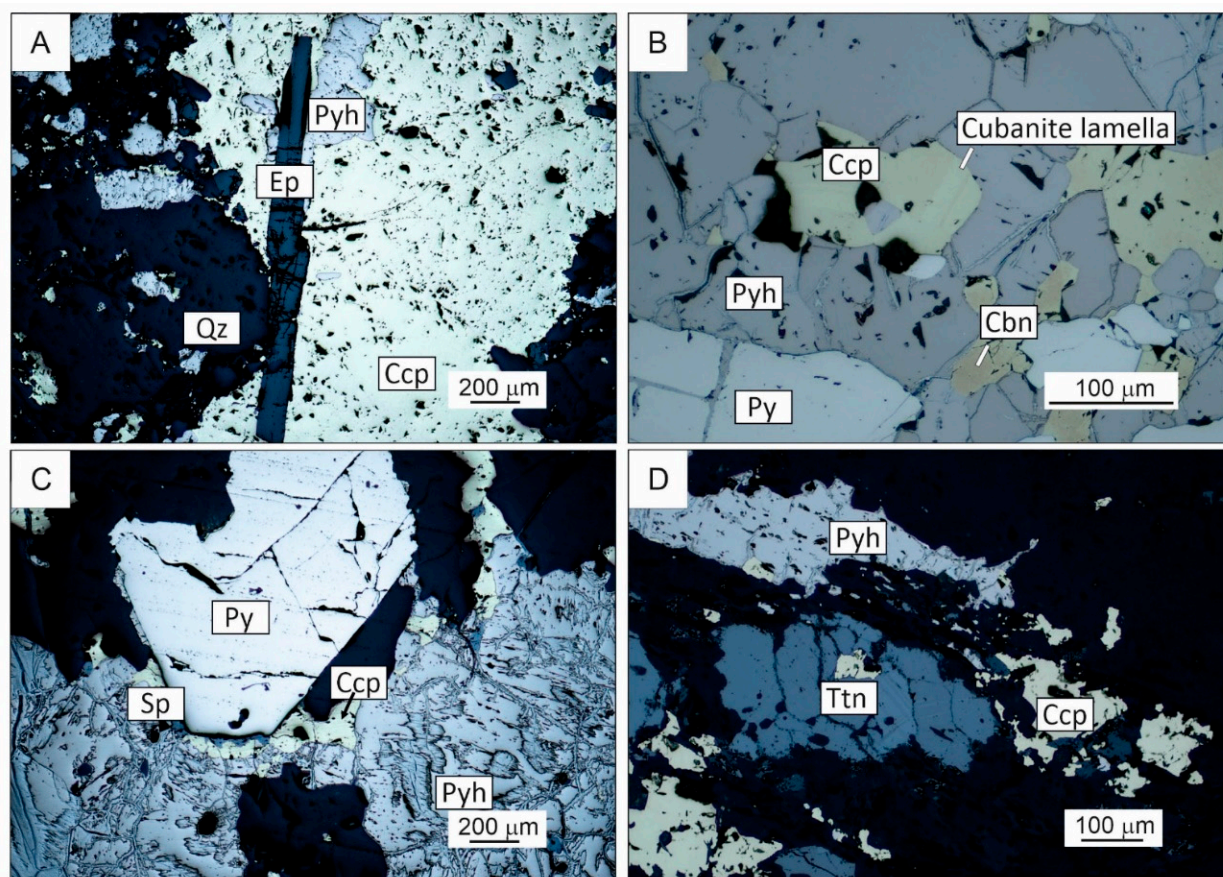
Figure 6. Reflected light microphotographs of the Alsvågen gabbro-hosted VMS mineralization: (**A**) Mineralization hosted by isotropic gabbro (PPL); (**B**) Massive sulfide mineralization hosted by the southern shear zone (PPL); (**C**) Massive sulfide mineralization hosted by the southern shear zone; (**D**) Hydrothermal veinlets hosted isotropic gabbro (PPL). Mineral abbreviations are according to [36]; Cbn—cubanite, Ccp—chalcopyrite, Ep—epidote, Py—pyrite, Pyh—pyrrhotite, Qz—quartz, Sp—sphalerite, Ttn—titanite.

Massive sulfide mineralization hosted by the shear zones consists mainly of pyrrhotite and chalcopyrite in association with variable amounts of pyrite and cubanite and minor amounts of sphalerite (Figure 6B,C). The textural features indicate post-ore deformation processes that led to brittle fragmentation of pyrite and ductile deformation of other sulfide phases (Figure 6B,C). Outside the shear zones, the mineralization occurs in the form of veinlets and dissemination. In both cases, pyrrhotite and chalcopyrite predominate, often accompanied by minor amounts of titanite (Figure 6D).

4.1.2. The Lindøya Basalt-Hosted VMS Mineralization

The VMS mineralization at Lindøya is hosted by basalts of the Lykling Ophiolite Complex (Figure 3B). Both barren and mineralized basalts consist of amphiboles, chlorites and weakly saussuritized plagioclases (Figure 7A). Lenses of massive sulfide mineralization show an intercalation of sulfide and silica layers. The sulfide layers are predominantly composed of pyrite and pyrrhotite, associated with minor amounts of chalcopyrite, magnetite and arsenopyrite (Figure 7B,C). Locally, younger generations of sulfides, mostly pyrite, crosscut the sulfide-silica layers. Disseminated mineralization is characterized by pyrite, chalcopyrite and minor amounts of sphalerite, often accompanied by extensive chloritization (Figure 7D).
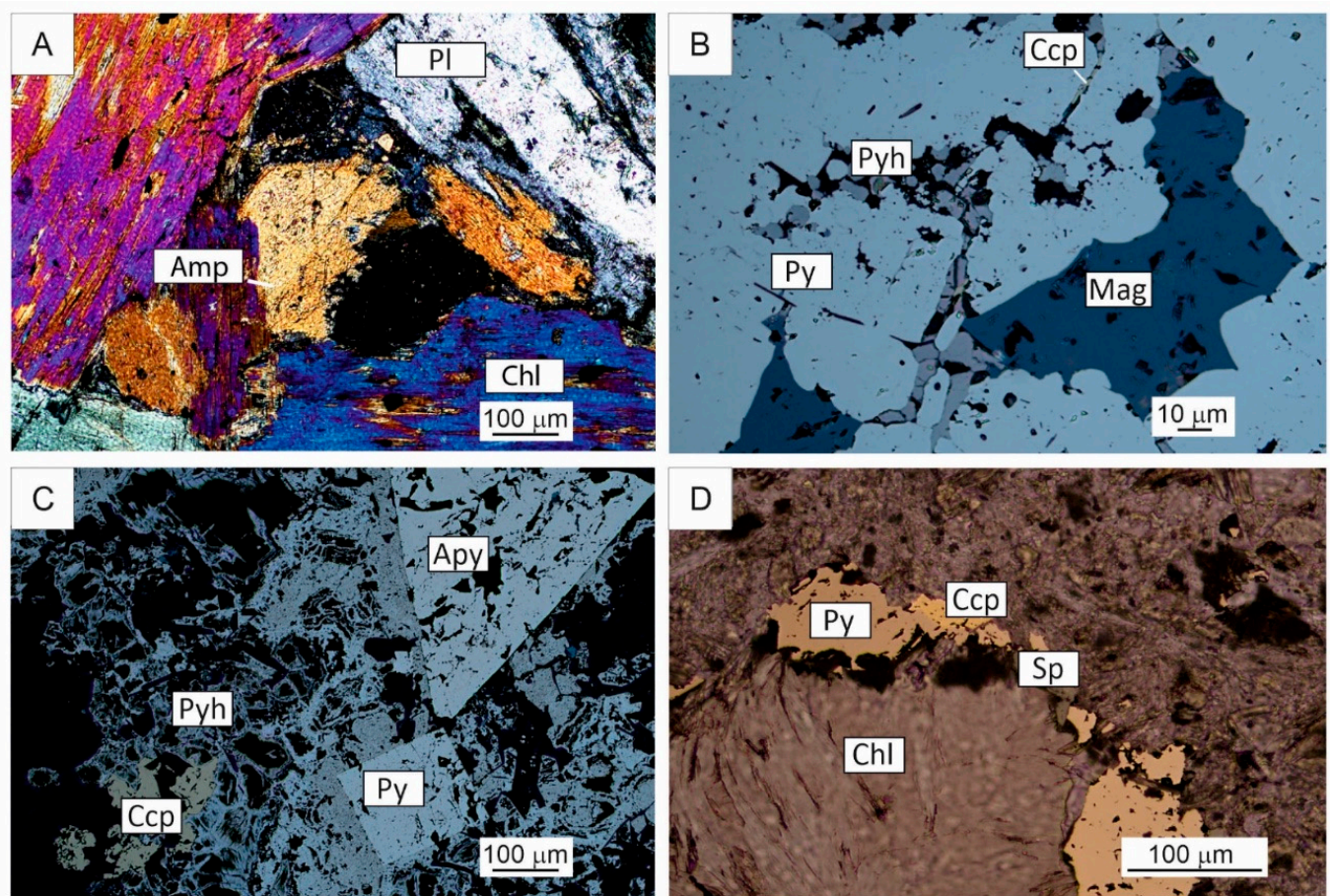
Figure 7. Microphotographs of the Lindøya basalt-hosted VMS mineralization: (**A**) Host basalt (transmitted light, PPL); (**B**) Massive sulfide mineralization (reflected light, PPL); (**C**) Massive sulfide mineralization (reflected light, PPL); (**D**) Disseminated sulfide mineralization (reflected light, PPL). Mineral abbreviations are according to [36]; Amp—amphibole, Apy—arsenopyrite, Ccp—chalcopyrite, Chl—chlorite, Mag—magnetite, Pl—plagioclase, Py—pyrite, Pyh—pyrrhotite, Sp—sphalerite.

4.1.3. The Litlabø Sediment-Hosted VMS Mineralization

The VMS mineralization at Litlabø is associated with a volcano–sedimentary complex composed of organic-rich black shales, layered siliciclastic sedimentary rocks, cherts and greenstones (Figure 3C). The intermediate host rock is finely laminated organic-rich black shale (Figure 4D,E).

Massive sulfide mineralization occurs in the form of bedding-parallel layers and can be subdivided into pyrite-rich mineralization and pyrrhotite-rich mineralization based on its mineral composition. The pyrite-rich sulfide mineralization consists of intercalated rhythmically altering layers composed of fine-grained porous pyrite (Py1) with layers composed of massive pyrite (Py2; Figure 8A). Only traces of pyrrhotite, chalcopyrite and sphalerite were observed. The mineralized layers are often crosscut by quartz veinlets a few millimeters thick. The pyrrhotite-rich sulfide mineralization consists of at least two generations of pyrrhotite. Early pyrrhotite is often associated with minor amounts of arsenopyrite and occurs in the form of fine-grained lamellas. These lamellas were subjected to extensive brecciation and afterwards cemented with the late generation of pyrrhotite (Figure 8B).
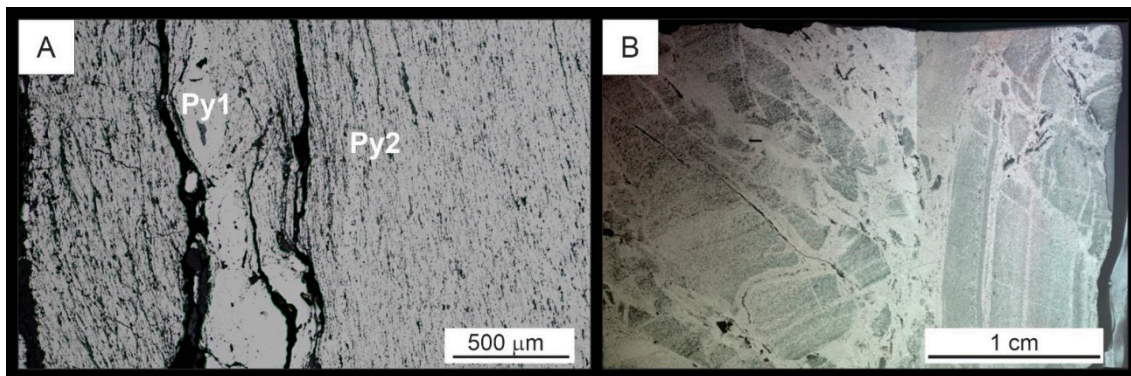
Figure 8. Microphotographs of the Litlabø sediment-hosted VMS mineralization: (**A**) Pyrite-rich sulfide mineralization consisting of at least two generations of pyrite (earlier Py1 and later Py; reflected light, PPL); (**B**) Pyrrhotite-rich sulfide mineralization reflects episodes of brecciation (thick section scan). Mineral abbreviations are according to [36]; Py—pyrite.

4.2. Ore Grade Analysis

The results of the ore grade analysis of representative massive sulfide samples collected from the Alsvågen, Lindøya and Litlabø VMS deposits as part of this study are shown in Table 1. Ore grade data from previous studies in the area are summarized in Table 2 [37].

The Alsvågen gabbro-hosted mineralization is characterized by a high Cu content, ranging from 1.2 to >10 wt.%. The mineralization is depleted in all other economically important elements. The Cu/(Zn+Pb) and Fe/base metal ratios range between ~40 and 300 and ~1.5 and 8, respectively (Tables 1 and 2; Figure 9). In contrast, the Lindøya basalt-hosted mineralization contains only 0.006 to 0.02 wt.% Cu. All other economically important elements are also depleted. The Cu/(Zn+Pb) ratio is <1, while the Fe/base metal ratio varies between ~400 and 1000 (Tables 1 and 2; Figure 9). The Litlabø-sediment hosted VMS mineralization contains between 0.02 and 0.11 wt.% Cu. The pyrrhotite-rich sample is enriched in Au, Ni and Co compared to the pyrite-rich sample. In general, the Litlabø mineralization is characterized by a low Cu/(Zn+Pb) ratio (<1.4) and a high Fe/base metal ratio (~200 to 500; Tables 1 and 2; Figure 9).
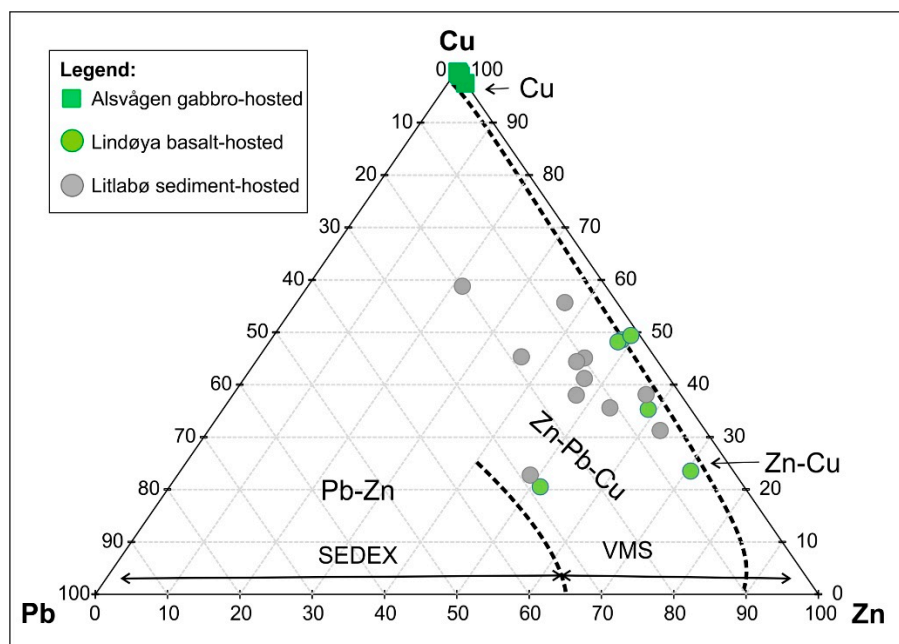
Figure 9. Base metal classification of the studied VMS deposits (after [5]).

Table 2. Previously published ore grade analysis from the Alsvågen, Lindøya and Litlabø VMS deposits, SW Norway *.

Sample	Element	Cu	Zn	Fe	Mn	S	Pb	Mo	As	Ni	Se	Tl	Ag	Au
	Unit			wt.%						ppm				ppb
The Alsvågen gabbro-hosted VMS deposit														
Alsvåg 01		3.77	0.04	20.10		8.52	2	7.72	3	74	118	*<d.l.* **	3.3	35
Alsvåg 02		2.94	0.02	11.56		3.57	4	4.00	3	13	45	*<d.l.*	2.6	46
The Lindøya basalt-hosted VMS deposit														
Lindøya 01		0.02	0.02	39.5		-	12	41.3	233	76	16	1	0.5	9
Lindøya 02		0.02	0.02	31.8		-	15	26.3	42	52	6	*<d.l.*	0.5	16
Lindøya 03		0.02	0.02	33.9		-	5	43.5	12	60	13	2	0.5	4
Lindøya 04		0.01	0.03	30.9		-	24	30.6	506	35	9	*<d.l.*	0.5	25
The Litlabø sediment-hosted VMS deposit														
HO0065.01		0.11	0.04	47.83	0.24	34.14	371	22	1412	341	-	-	0.8	284
HO0065.02		0.05	0.04	31.18	0.88	34.39	203	9	1027	142	-	-	1.2	160
HO0065.03		0.06	0.04	33.03	0.77	27.63	78	13	470	103	-	-	0.3	27
HO0065.04		0.02	0.04	27.73	0.61	35.21	40	5	571	74	-	-	0.3	22
HO0065.05		0.02	0.03	24.71	1.76	11.19	25	10	430	41	-	-	1.4	7
HO0065.06		0.06	0.06	47.11	0.08	33.72	130	24	729	129	-	-	*<d.l.*	25
HO0065.07		0.02	0.03	27.83	0.10	40.75	62	4	684	81	-	-	0.4	26
HO0065.08		0.04	0.05	44.11	0.08	34.70	152	18	744	130	-	-	*<d.l.*	39
HO0065.09		0.03	0.03	26.39	0.40	33.89	76	9	843	110	-	-	0.3	32

*—data from the Norwegian Geological Survey mineral resource database; ** < *d.l.*—below detection limit.

4.3. Trace Element Composition of Sulfide Minerals

The trace element composition of selected sulfide phases from the Alsvågen, Lindøya and Litlabø VMS deposits is listed in Appendix A and illustrated in Figure 10.
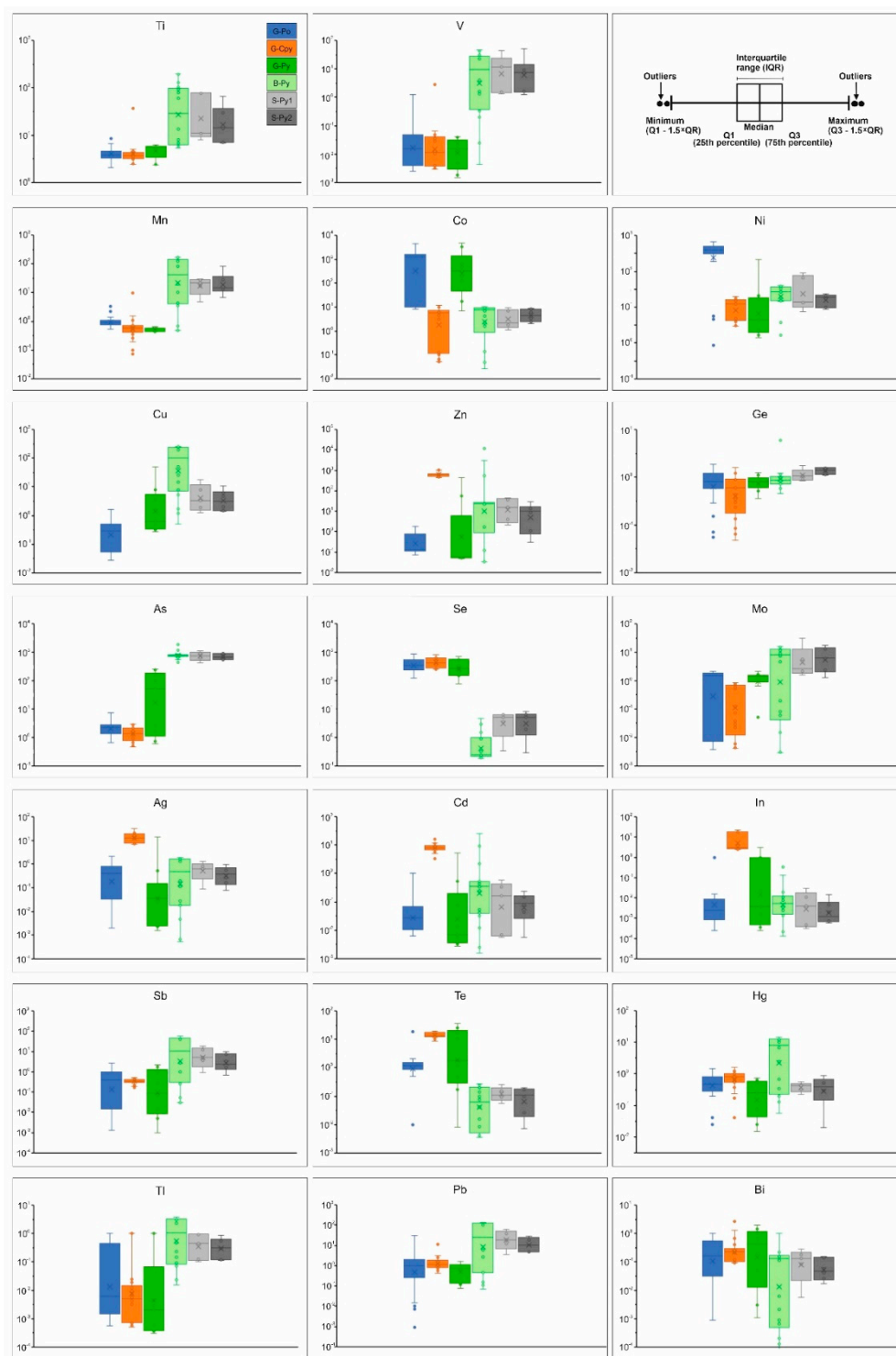
Figure 10. Box and whisker plots for a selected range of trace elements measured in pyrrhotite, pyrite and chalcopyrite from the Alsvågen gabbro-, Lindøya basalt- and Litlabø sediment-hosted VMS deposits. Abbreviations: G-Po: gabbro-hosted pyrrhotite; G-Py: gabbro-hosted pyrite; G-Py: gabbro-hosted chalcopyrite; B-Py: basalt-hosted pyrite; S-Py: sediment-hosted pyrite.

Sulfide minerals (pyrite, pyrrhotite and chalcopyrite) from the gabbro-hosted Alsvågen VMS mineralization are enriched in Se and Te and depleted in Ti, V, Mn, As, Sb, Tl and Pb compared to pyrite from the basalt-hosted Lindøya and the sediment-hosted Litlabø VMS deposits (Figure 10). Sulfides of the Alsvågen VMS mineralization are also characterized by high Se/As, Se/Tl and Se/S ratios compared to sulfides from the latter two deposits (Appendix A). The Alsvågen pyrrhotite is enriched in Co (8.5–4651.0 ppm, with a mean value of 1251.5 ppm) and Ni (0.9–680.9 ppm, with a mean value of 375.7 ppm). In contrast, chalcopyrite from Alsvågen is enriched in Zn (442.5–1062.2 ppm, with a mean value of 643.6 ppm), Ag (7.0–31.0 ppm, with a mean value of 13.7 ppm), Cd (3.3–15.9 ppm, with a mean value of 8.3 ppm) and In (2.4–23.2 ppm, with a mean value of 8.2 ppm).

The comparison of the trace element composition of the pyrite from the investigated VMS deposits revealed that the gabbro-hosted pyrite is depleted in most of the analyzed elements, with the exception of Co, Se, Te, In and Bi (Figure 10). The gabbro-hosted pyrite is characterized by Se/As and Se/Tl ratios in the ranges between ~0.6 and 285 (a mean value of 82) and $>5*10^6$, respectively. Its $Se/S*10^6$ value spans between 131 and 1650 (a mean value of 672; Appendix A). The basalt-hosted pyrite exhibits elevated contents of As (450.2–1907.7 ppm, with a mean value of 827.9 ppm), Cu (0.5–257.9 ppm, with a mean value of 123.1 ppm), Mn (0.5–170.5 ppm; 73.6 ppm), Pb (0.1–135.0 ppm, with a mean value of 61.8 ppm), Ti (5.4–200.9 ppm, with a mean value of 61.4 ppm), Sb (<56.9 ppm, with a mean value of 24.3 ppm), Hg (<14.7 ppm, with a mean value of 6.9 ppm) and Tl (<3.8 ppm, with a mean value of 1.6 ppm). The sediment-hosted pyrite shows an enrichment in As (Py1: 423.2–1104.2 ppm, with a mean value of 769.9 ppm; Py2: 553.0–919.0 ppm, with a mean value of 713.0 ppm), Pb (Py1: 3.5–64.3 ppm, with a mean value of 27.3 ppm; Py2: 4.8–29.3 ppm, with a mean value of 14.3 ppm); Mo (Py1: 1.6–30.6 ppm, with a mean value of 8.6 ppm; Py2: 1.3–17.6 ppm, with a mean value of 7.9 ppm), Ge (Py1: 0.8–1.7 ppm, with a mean value of 1.1 ppm; Py2: 1.1–1.6 ppm, with a mean value of 1.4 ppm) and Tl (Py1: 0.1–1.0 ppm, with a mean value of 0.5 ppm; Py2: 0.1–0.9 ppm, with a mean value of 0.4 ppm).

4.4. Sulfur Isotopes

The sulfur isotope composition of sulfide phases from the VMS deposits Alsvågen, Lindøya and Litlabø is shown in Table 3 and graphically presented in Figure 11. Sulfide minerals from the Alsvågen gabbro-hosted deposit show a range of $\delta^{34}S$ values between 0.4 and 3.9 ‰ VCDT (n = 12, with a mean value of 1.6 ‰, as shown in Table 3). The sulfides from the Lindøya basalt-hosted are characterized by $\delta^{34}S$ values between 4.9 and 5.9 ‰ VCDT (n = 5, with a mean value of 5.4 ‰, as shown in Table 3). The Litlabø sediment-hosted sulfides exhibit a significant depletion of ^{34}S and show $\delta^{34}S$ values between −19.7 and −15.7 ‰ VCDT (n = 4; mean = −17.6 ‰; Table 3).

Table 3. Sulfur isotope ($\delta^{34}S$) composition of sulfide minerals from the Alsvågen, Lindøya and Litlabø VMS deposits, SW Norway.

Sample	Mineralogy	$\delta^{34}S$ (VCDT, ‰)
The Alsvågen gabbro-hosted VMS deposit		
20ALS3S1	Pyrite	0.5
20ALS3S2-po1	Pyrite	3.9
20ALS3S2-po2	Pyrite	0.4
20ALS4E	Pyrite	1.8
20ALS4F	Pyrite	3.0
20ALS7S1-po2	Pyrite	2.4
20ALS7S3-po1	Pyrite	1.4
20ALS7S3-po2	Pyrite	1.6
20ALS6D1-po1	Pyrite	1.5
20ALS6D1-po2	Pyrite	0.6
20ALS6D2	Pyrite	1.8
20ALS10B	Chalcopyrite	0.9

Table 3. *Cont.*

Sample	Mineralogy	$\delta^{34}S$ (VCDT, ‰)
The Lindøya basalt-hosted VMS deposit		
20LIND-H	Pyrite	4.9
20LIND4B-po1	Pyrite	5.9
20LIND4B-po2	Pyrite	5.7
20LIND4B-po3	Pyrrhotite	5.9
20LIND4B-po4	Pyrrhotite	5.7
The Litlabø sediment-hosted VMS deposit		
19LIT2-po1	Pyrite	−19.3
19LIT2-po2	Pyrite	−19.7
19LIT3-po1	Pyrrhotite	−15.8
19LIT3-po2	Pyrrhotite	−15.7
19LIT3-po2	Pyrrhotite	−15.7
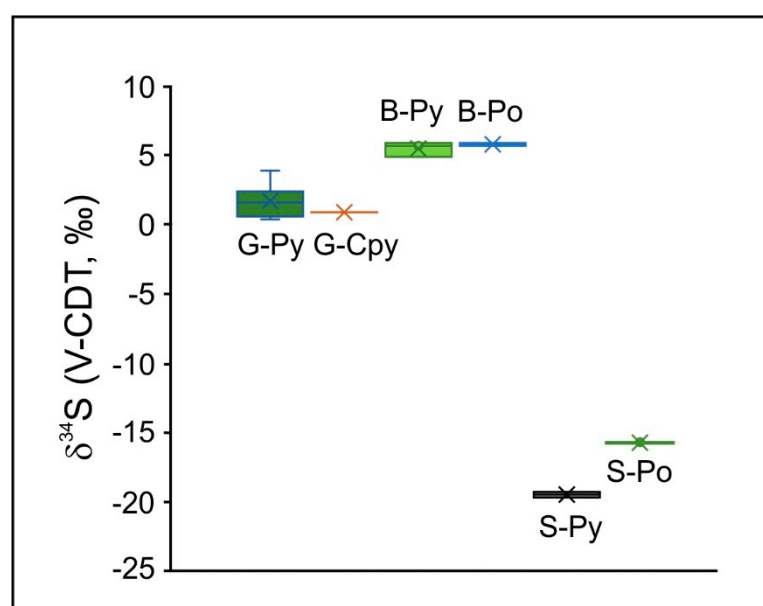
Figure 11. Box and whisker plots for illustrating the $\delta^{34}S$ composition of sulfides from the Alsvågen gabbro-, Lindøya basalt- and Litlabø sediment-hosted VMS deposits. Abbreviations: G–Py: gabbro-hosted pyrite; G–Cpy: gabbro-hosted chalcopyrite; B–Py: basalt-hosted pyrite; B–Po: basalt-hosted pyrrhotite; S–Py: sediment-hosted pyrite; S–Po: sediment-hosted pyrrhotite.

5. Discussion

Although all of the VMS deposits indicate that they are products of hydrothermal activity within the seafloor, they can be a source of different commodities (e.g., Cu-Zn-rich, Cu-Zn-Pb-rich, Cu-Zn-Au-rich, Cu-Zn-Co-rich, etc.; [5]) and may have variable economic potential depending on their initial geological setting and the local physicochemical conditions during their formation as well as during the tectonic transport and obduction of the seafloor onto the continental crust (e.g., [38]). In addition, deeper parts of ophiolite sequences may host massive sulfides related to primary magmatic processes [39–42].

Recent developments in microbeam analytical methods, including the in situ LA-ICP-MS technique, enable the determination of trace element distributions in individual mineral phases, including sulfides (e.g., [43–46]). The trace element content of pyrite, the most common sulfide mineral in various types of mineral deposits, is considered to be an important source of information on the depositional mechanisms of sulfide in both magmatic and hydrothermal deposits (e.g., [47–50]). Several studies on VMS deposits suggest that the trace element content of pyrite can also be used as a vector in the exploration of this type of deposit (e.g., [51–53]).

In this study, we selected three massive sulfide deposits from the Sunnhordland region in SW Norway hosted by different lithologies to test the effectiveness of trace element and $\delta^{34}S$ signatures of sulfide phases in distinguishing VMS deposits in different geological settings. The Alsvågen gabbro-hosted VMS deposit is characterized by a high Cu grade (1.2 to >10 wt.%) and an abundance of chalcopyrite and cubanite associated with pyrrhotite, pyrite and sphalerite (Figure 6; Tables 1 and 2). In contrast, the Lindøya basalt-hosted VMS deposit is characterized by a high Fe/base metal ratio and a Cu grade ranging between 0.006 and 0.02 wt.% (Figure 7; Tables 1 and 2). The main sulfide phases are pyrite and pyrrhotite. The Litlabø sediment-hosted VMS deposit also has a low Cu grade (0.02–0.11 wt.%), with pyrite and pyrrhotite being the main sulfide minerals. The pyrrhotite-rich mineralization is slightly enriched in Au, Ni and Co (Figure 8; Tables 1 and 2).

Pyrite from the Alsvågen gabbro-hosted VMS deposit shows a considerable enrichment in Co, Se, Te, In and Bi compared to pyrite from the Lindøya basalt-hosted and Litlabø sediment-hosted VMS deposits. In contrast, pyrite from the latter two deposits is enriched in V, Mn, As, Sb, Tl and Pb (Appendix A; Figure 10). Previous studies on the trace element characteristics of pyrite from VMS deposits indicated a significant negative correlation between As and Se in hydrothermal pyrite, presumably controlled by their competition for S site and fluid temperature [51]. The Se/Tl ratio has also been proposed as an indicator of fluid temperature and can be used directly to distinguish between mineralized and barren zones in VMS prospects [51,54]. The high Se/As and Se/Tl ratios recorded from the gabbro-hosted pyrite indicate a relatively high formation temperature for the Alsvågen mineralization and clearly distinguish the high-grade gabbro-hosted mineralization from the low-grade basalt-hosted and sediment-hosted types of VMS mineralization. The high Se/S ratio in the Alsvågen pyrite (Se/S*10^6 = 131–1650, with a the mean value of 672) indicates an influx of magmatic volatiles (e.g., [55–57]). The Co/Sb vs. Se/As ratios support the magmatic affinity of the Alsvågen mineralization (Figure 12; [45,58]).
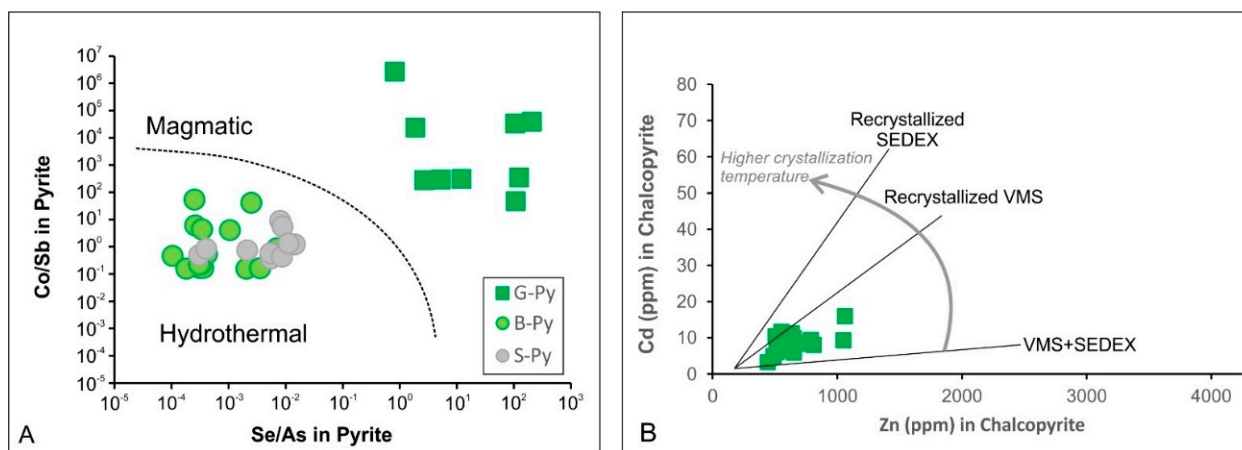
Figure 12. (**A**) The Co/Sb vs. Se/As diagram [45,58] showing a contrasting trace element signature of pyrite from the Alsvågen gabbro-hosted deposit (G–Py) compared to pyrite from the Lindøya basalt-hosted (B–Py) and the Litlabø sediment-hosted (S–Py) deposits; (**B**) Cd vs. Zn contents of chalcopyrite from the Alsvågen gabbro-hosted deposit.

Pyrite from the Lindøya basalt-hosted and Litlabø sediment-hosted VMS deposits overlap considerably in terms of trace element composition (Figure 10); therefore, the binary trace element plots cannot be used for their discrimination (Figure 13). In contrast to pyrite from the gabbro-hosted Alsvågen mineralization, pyrite from Lindøya and Litlabø reflects a hydrothermal affinity in the Co/Sb vs. Se/As diagram (Figure 12A; [45,58]).
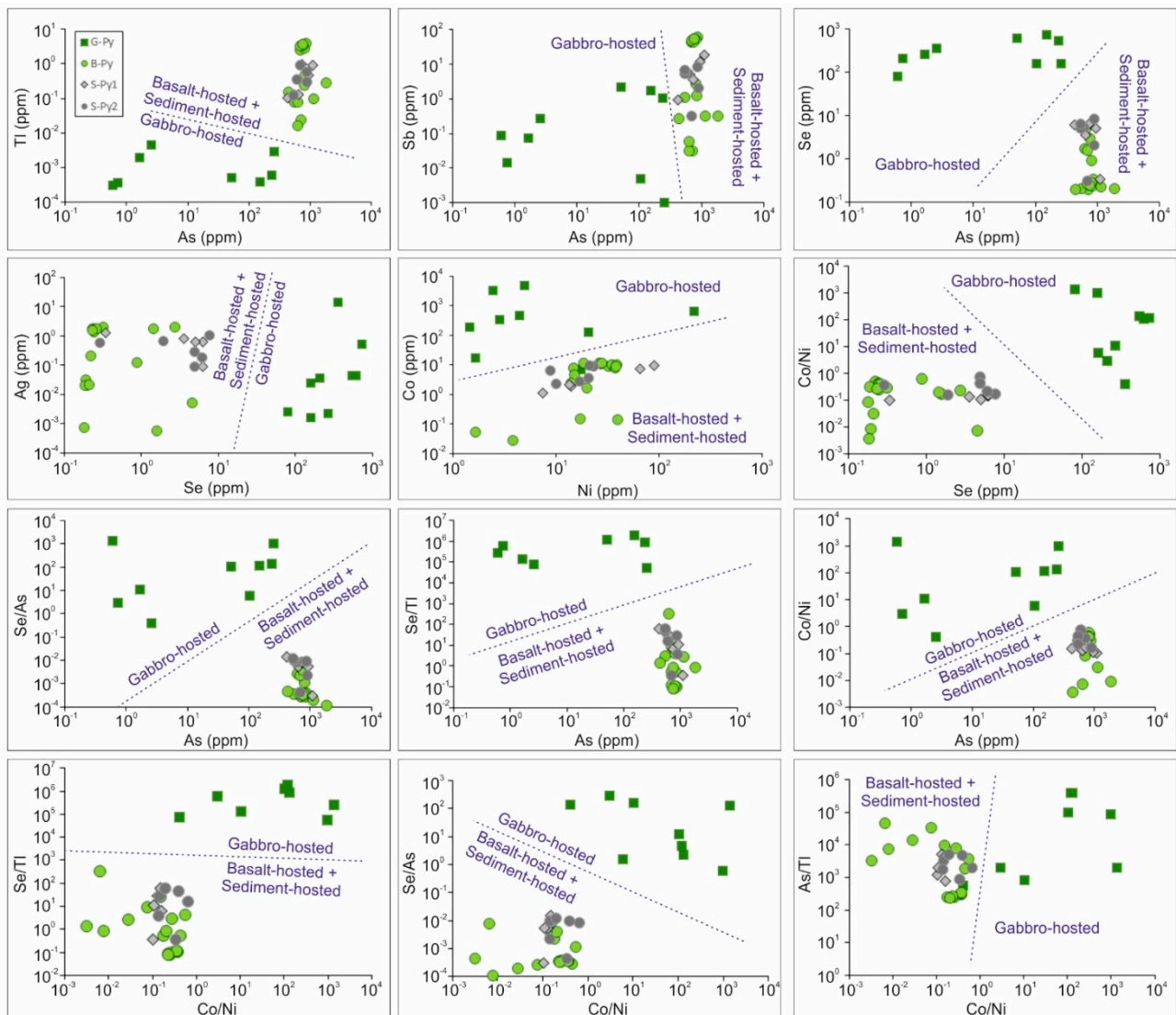
Figure 13. Discrimination binary diagrams based on the trace element composition of pyrite from the Alsvågen gabbro-, Lindøya basalt- and Litlabø sediment-hosted VMS deposits. Abbreviations: G–Py: gabbro-hosted pyrite; B–Py: basalt-hosted pyrite; S–Py: sediment-hosted pyrite.

Chalcopyrite and pyrrhotite from the Alsvågen VMS deposit were also analyzed for their trace element content. The recorded enrichments of chalcopyrite in Se, Ag, Zn, Cd and In and of pyrrhotite in Ni and Co (Appendix A; Figure 10) are probably controlled by the partition of trace elements between coprecipitating sulfide phases (e.g., [59–62]). The Zn vs. Cd content of chalcopyrite reflects that the Alsvågen mineralization has been subjected to post-formation recrystallization processes at elevated temperatures (Figure 12B; [45]).

Sulfide mineralization from the studied VMS deposits in the Sunnhordland region, SW Norway, shows a distinct $\delta^{34}S$ signature (Table 3, Figure 11). The Alsvågen gabbro-hosted mineralization is characterized by $\delta^{34}S$ values between 0.4 and 3.9 ‰ VCDT (n = 12, with a mean value of 1.6 ‰, as shown in Table 3), indicating a magmatic contribution of sulfur (e.g., [63]).

The Lindøya basalt-hosted mineralization shows $\delta^{34}S$ values ranging between 4.9 and 5.9 ‰ VCDT (n = 5, with a mean value of 5.4 ‰, as shown in Table 3). These values are similar to the sulfur isotope composition of sulfide minerals from the basalt-hosted VMS deposits elsewhere (e.g., [64–66]). Pyrite with Se/S*10^6 values of <11.5 reflects a negligible contribution from magmatic volatiles, additionally supporting the notion that sulfur at Lindøya was predominantly leached from the host basalt.

The Litlabø sediment-hosted mineralization with $\delta^{34}S$ values between -19.7 and -15.7 ‰ VCDT (n = 4; mean = -17.6 ‰; Table 3) reflects the bacterial reduction of marine sulfate as the main source of sulfur in this deposit (e.g., [67,68]). The low Se/S*10^6 values measured in pyrite (<14.9) are consistent with a non-magmatic source of sulfur.

The distinctive sulfur isotope signature of pyrite from the three examined types of VMS deposits can be used to distinguish gabbro-, basalt- and sediment-hosted VMS deposits. As illustrated in Figure 14, the combination of characteristic $\delta^{34}S$ ranges with trace element attributes provides a robust tool for the differentiation of pyrite from VMS deposits hosted by different lithologies. Therefore, the proposed binary $\delta^{34}S$ trace element plots have a strong potential for use in discriminating provenances of individual pyrite grains extracted from stream sediments, soils or till material.
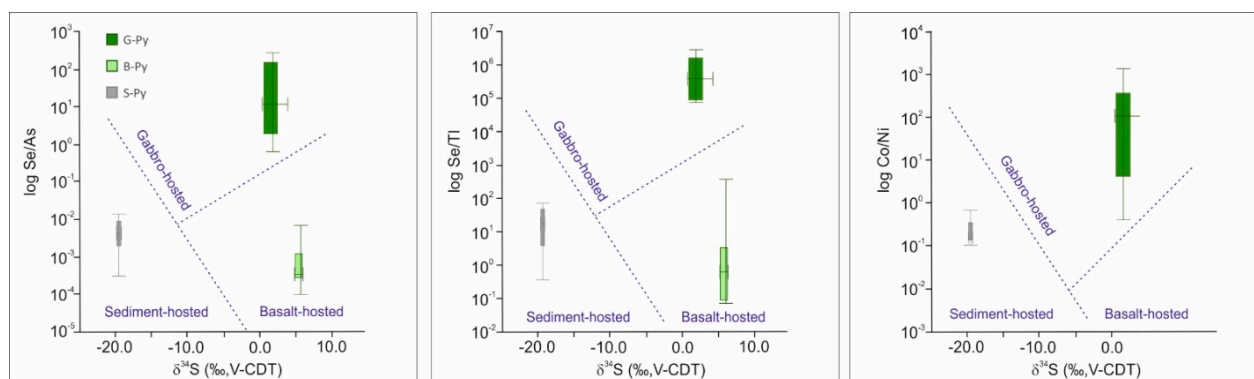
Figure 14. Discrimination binary diagrams based on the trace element and $\delta^{34}S$ composition of pyrite from the Alsvågen gabbro-, Lindøya basalt- and Litlabø sediment-hosted VMS deposits. Abbreviations: G–Py: gabbro-hosted pyrite; B–Py: basalt-hosted pyrite; S–Py: sediment-hosted pyrite.

6. Conclusions

Despite their abundance and diversity, the VMS deposits of the Sunnhordland region, SW Norway, have not been subjected to previous mineralogical, geochemical or stable isotope investigations. This study brings an overview of mineral characteristics of the VMS deposits hosted by different lithologies, including gabbro and basalt of the Lykling Ophiolite Complex, as well as organic-rich sediments of the Langevåg Group, coupled with new trace element and $\delta^{34}S$ data obtained sulfide mineral phases.

The Alsvågen gabbro-hosted VMS mineralization (1.2 to >10 wt.% of Cu) consists of chalcopyrite and cubanite in association with pyrrhotite, pyrite and sphalerite. Pyrite has a significant enrichment of Co (7–4867 ppm, with an average value of 1105 ppm), Se (80–723 ppm, with an average value of 345 ppm) and Te (<36 ppm, with an average value of 12 ppm). The high Se/As and Se/Tl ratios reflect a relatively high formation temperature for Alsvågen mineralization, while the high Se/S ratio (Se/S*10^6 = 131–1650, with a mean value of 672) suggests a contribution from magmatic volatiles. The $\delta^{34}S$ values of sulfide phases that range within the interval from 0.4 to 3.9 ‰ VCDT (n = 12, with a mean value of 1.6 ‰) additionally support a significant influx of magmatic sulfur. Chalcopyrite from the Alsvågen VMS shows enrichment of Se, Ag, Zn, Cd and In, while pyrrhotite concentrates Ni and Co.

The Lindøya basalt-hosted VMS mineralization (0.006 to 0.02 wt.% of Cu) consists predominantly of pyrite and pyrrhotite. Pyrite is enriched in As (450–1908 ppm, with an average value of 828 ppm), Mn (0.03–171 ppm, with an average value of 74 ppm), Pb (0.07–135 ppm, with an average value of 62 ppm), Sb (0.03–57 ppm, with an average value of 24 ppm), V (0.5–48 ppm, with an average value of 16 ppm) and Tl (0.02–4 ppm, with an average value of 2 ppm). The $\delta^{34}S$ values of sulfides range between 4.9 and 5.9 ‰ VCDT (n = 5, with a mean value of 5.4 ‰). These values, together with the Se/S ratio in pyrite (Se/S*10^6 values <11.5), suggest that the sulfur at Lindøya was predominantly leached from the host basalt.

The Litlabø sediment-hosted VMS mineralization (0.02–0.11 wt.% of Cu) also consists predominantly of pyrite and pyrrhotite. Pyrite is enriched in the same suite of elements as pyrite from Lindøya (As (423–1104 ppm, with an average value of 739 ppm), Mn (5–82 ppm, with an average value of 24 ppm), Pb (4–64 ppm, with an average value of 20 ppm), V (1–52 ppm, with an average value of 14 ppm), Sb (0.7–19 ppm, with an average value of 6 ppm) and Tl (0.1–1 ppm, with an average value og 0.5 ppm). The Litlabø sediment-hosted mineralization has $\delta^{34}S$ values between –19.7 and –15.7‰ VCDT, indicating that the bacterial reduction of marine sulfate is the main source of sulfur in this deposit. The low $Se/S*10^6$ values measured in pyrite (<14.9) support a non-magmatic source of sulfur.

Trace element characteristics, in particular Tl, Sb, Se, As, Co and Ni concentrations and their mutual ratios have been identified as an efficient tool to distinguish the gabbro-hosted VMS mineralization from the basalt- and sediment-hosted types of VMS mineralization. The trace element features of pyrite, coupled with its distinctive sulfur isotope signature, represent a novel and robust tool for distinguishing gabbro-, basalt- and sediment-hosted VMS mineralization.

Appendix A

Table A1. Trace element composition (LA-ICP-MS) of sulfide phases from the Alsvågen, Lindøya and Litlabø VMS deposits, SW Norway.

Sample	Mineral	S	Ti	V	Cr	Mn	Co	Ni	Cu	Zn	Ge	As	Se	Mo	Ag	Cd	In	Sb	Te	Au	Hg	Tl	Pb	Bi
																			(ppm)					

The Alsvågen gabbro-hosted VMS deposit

Sample	Mineral	S	Ti	V	Cr	Mn	Co	Ni	Cu	Zn	Ge	As	Se	Mo	Ag	Cd	In	Sb	Te	Au	Hg	Tl	Pb	Bi
20ALS4F	Pyrrhotite	425,296	3.69	0.017	<0.195	0.88	2097.25	669.64	0.113	<0.17	1.16	2.63	349.18	2.190	0.584	0.082	0.0063	0.133	0.964	<0.001	0.320	0.009	1.236	0.149
20ALS4F	Pyrrhotite	422,777	3.17	0.114	2.43	2.17	2276.11	674.51	1.671	0.93	0.15	3.15	335.35	1.679	0.730	0.101	<0.0001	2.630	1.519	<0.001	0.210	0.012	2.070	0.260
20ALS4F	Pyrrhotite	417,103	3.82	<0.007	1.58	2.64	2032.58	680.85	0.132	1.78	<0.11	3.53	331.61	1.636	0.378	0.073	<0.0010	0.340	0.730	<0.001	0.410	<0.00	0.268	0.046
20ALS4F	Pyrrhotite	468,275	3.63	<0.008	0.64	0.80	1662.66	648.78	<0.115	<0.23	0.29	2.02	389.42	1.910	0.154	<0.025	0.0049	0.013	1.217	<0.001	0.450	<0.002	0.133	0.031
20ALS4F	Pyrrhotite	442,520	4.60	0.049	<0.225	0.85	1484.45	620.39	<0.094	<0.25	<0.14	2.41	370.53	1.890	0.823	0.020	<0.0016	0.780	1.630	<0.001	0.260	<0.001	0.981	0.300
20ALS4F	Pyrrhotite	458,540	3.99	<0.007	3.28	0.79	1617.11	657.11	<0.102	0.81	1.31	3.58	367.53	1.970	0.577	<0.022	0.0026	0.349	1.156	<0.001	0.650	<0.002	0.404	0.125
20ALS3S1	Pyrrhotite	398,144	4.47	0.046	2.34	0.99	8.45	376.40	0.487	<0.20	0.16	1.97	255.79	1.230	0.078	<0.018	0.0072	<0.001	0.917	<0.001	0.750	0.004	0.007	<0.0018
20ALS3S1	Pyrrhotite	407,353	2.92	<0.008	1.97	1.10	10.15	431.49	0.322	1.59	1.23	2.91	243.67	2.120	0.025	0.042	0.0156	<0.001	1.055	0.004	0.670	0.003	<0.002	0.026
20ALS3S1	Pyrrhotite	416,228	5.22	<0.006	2.49	0.85	10.37	308.50	<0.087	<0.21	1.00	2.60	261.34	1.920	2.090	<0.025	0.0023	<0.004	1.840	<0.001	1.310	<0.001	4.470	0.550
20ALS3S1	Pyrrhotite	786,358	6.71	0.028	<0.13	0.65	3616.34	0.87	0.477	<0.15	0.84	7.07	128.44	1.512	0.011	0.034	0.0099	<0.001	<0.021	<0.001	<0.050	<0.001	<0.001	<0.00
20ALS3S1	Pyrrhotite	819,632	9.38	0.158	<0.14	0.95	3765.96	4.64	1.223	<0.16	1.02	0.66	138.48	1.810	0.019	0.053	<0.0005	<0.003	0.510	<0.001	0.200	<0.001	0.010	0.560
20ALS3S1	Pyrrhotite	874,963	8.43	0.013	<0.12	0.68	4650.96	5.64	0.255	1.15	0.61	1.05	169.81	2.140	<0.004	0.089	<0.0001	<0.001	<0.020	<0.001	0.270	0.005	<0.001	<0.00
20ALS3S1	Pyrrhotite	432,864	2.92	<0.009	0.60	0.65	9.98	405.21	1.092	<0.24	0.66	2.79	287.39	1.930	0.675	<0.023	<0.0018	0.042	1.820	<0.001	0.810	0.004	1.135	0.530
20ALS3S1	Pyrrhotite	410,557	2.08	0.041	2.66	1.26	9.46	537.51	0.425	0.43	1.86	2.72	260.94	1.470	0.033	<0.0139	0.0016	<0.001	1.730	<0.001	0.480	0.003	0.015	0.005
20ALS3S1	Pyrrhotite	412,967	2.06	0.033	1.95	0.88	10.19	266.44	0.204	0.49	0.92	2.94	246.45	1.570	0.455	<0.0129	0.0021	<0.001	1.039	<0.001	0.460	<0.001	0.257	0.170
20ALS3S1	Pyrrhotite	417,885	3.05	<0.005	4.56	0.81	10.14	361.24	0.548	1.16	1.22	1.87	243.42	1.680	1.430	<0.015	<0.0001	<0.001	0.938	<0.001	1.290	0.038	6.640	0.390
20ALS3S1	Pyrrhotite	452,905	4.11	<0.010	2.46	0.59	10.42	441.11	0.464	<0.31	0.75	2.54	244.58	1.770	0.425	0.075	<0.0023	<0.001	1.420	<0.001	0.810	<0.001	0.317	0.210
20ALS3S1	Pyrrhotite	445,247	3.36	0.029	0.89	0.91	9.83	402.16	0.516	<0.25	1.24	2.77	247.57	1.540	0.893	0.025	0.0024	0.009	0.944	<0.01	1.480	0.003	0.458	0.150
20ALS4E	Pyrrhotite	347,574	4.19	<0.010	<0.28	1.43	1304.18	350.31	<0.065	0.70	1.38	2.51	561.48	<0.011	0.873	0.196	0.0089	0.046	1.400	<0.001	0.500	<0.001	3.780	0.118
20ALS4E	Pyrrhotite	337,446	3.27	<0.006	1.81	0.79	1245.77	333.94	0.075	0.54	0.80	1.07	698.23	<0.012	0.753	0.030	0.0020	0.008	1.180	<0.001	0.480	0.008	5.160	0.227
20ALS4E	Pyrrhotite	337,265	3.67	0.009	<0.26	0.57	1334.37	301.14	0.523	1.46	0.79	1.41	609.65	<0.013	1.560	0.029	0.0034	0.035	2.130	<0.001	0.840	0.007	8.660	1.040
20ALS4E	Pyrrhotite	341,799	3.87	0.053	3.03	0.52	1337.99	415.51	<0.056	<0.23	0.78	1.22	441.96	0.072	1.640	0.015	<0.0001	<0.001	0.830	<0.001	0.830	0.008	1.480	0.125
20ALS4E	Pyrrhotite	324,296	5.23	0.074	<0.27	0.98	1071.13	397.18	<0.076	<0.23	0.59	1.22	571.34	<0.008	0.006	<0.0124	0.0032	<0.001	0.880	<0.001	1.430	<0.001	<0.001	<0.00
20ALS4E	Pyrrhotite	347,078	4.45	0.015	3.58	1.11	1372.66	227.16	0.762	<0.25	0.57	1.30	874.34	<0.011	0.343	<0.016	<0.0009	0.440	18.920	<0.001	0.430	<0.001	29.960	0.750
20ALS4E	Pyrrhotite	351,498	3.85	0.022	<0.30	0.76	1290.67	191.36	0.252	<0.26	1.29	1.60	793.44	<0.017	0.035	<0.00	<0.0012	0.008	1.200	<0.001	0.200	<0.002	<0.001	0.002
20ALS4E	Pyrrhotite	330,721	4.12	0.059	1.27	0.78	1203.75	361.85	0.480	<0.23	1.33	1.54	500.18	<0.013	0.032	0.039	<0.0008	0.021	0.730	<0.001	0.460	0.004	0.009	0.003
20ALS4E	Pyrrhotite	322,435	3.90	<0.008	5.09	0.92	1142.70	345.13	<0.079	<0.24	0.82	1.74	706.50	0.044	0.064	0.021	<0.0009	<0.003	1.500	<0.001	0.390	<0.002	0.343	0.012
20ALS4E	Pyrrhotite	334,975	5.59	1.230	3.03	3.40	1291.24	396.96	0.334	0.48	0.42	0.85	478.60	<0.014	0.237	0.060	0.0044	<0.001	1.200	<0.001	0.610	0.008	1.950	0.032
20ALS4E	Chalcopyrite	304,609	3.99	<0.008	0.26	0.07	9.93	5.43	251,939.440	487.70	1.24	0.75	639.29	<0.009	8.490	4.930	2.4600	0.226	8.550	<0.001	0.820	0.025	2.540	0.108
20ALS4E	Chalcopyrite	297,739	4.63	0.010	2.45	0.59	7.71	2.92	237,609.660	788.17	0.60	0.68	579.53	0.029	8.800	9.380	2.5800	0.320	10.060	<0.001	0.560	0.009	3.150	0.234
20ALS4E	Chalcopyrite	296,910	3.75	0.052	2.46	0.57	5.00	3.33	263,605.380	442.48	0.43	1.29	537.98	0.117	8.510	3.310	2.3800	0.410	12.220	<0.001	0.620	0.019	1.960	0.120
20ALS4E	Chalcopyrite	296,795	3.06	0.057	3.33	0.26	3.21	3.05	256,279.840	651.45	0.36	1.32	493.13	<0.008	7.240	5.890	2.6500	0.260	12.500	<0.001	0.170	<0.001	0.810	0.092
20ALS4E	Chalcopyrite	312,468	4.45	0.047	2.41	0.45	7.69	4.77	280,534.630	618.09	0.96	0.66	836.32	0.072	7.380	7.190	2.7800	0.340	13.610	0.004	<0.084	0.005	0.850	0.104
20ALS4E	Chalcopyrite	319,662	4.29	<0.007	0.60	0.66	4.74	4.27	264,177.060	720.11	0.63	0.45	769.43	<0.010	7.910	8.390	2.7400	0.189	11.170	<0.001	0.970	<0.001	0.755	0.095
20ALS4E	Chalcopyrite	310,958	4.09	0.029	<0.23	0.72	5.60	4.25	260,726.250	809.55	0.91	0.51	676.36	<0.013	7.360	8.000	2.7900	0.340	14.980	<0.001	0.380	<0.001	0.940	0.093
20ALS4E	Chalcopyrite	296,761	4.37	<0.007	1.29	1.56	4.54	3.84	253,637.610	542.39	0.30	1.34	651.84	0.022	7.350	6.690	2.5900	0.340	13.020	<0.0019	0.730	0.011	1.750	0.105
20ALS4E	Chalcopyrite	301,785	2.51	<0.007	1.18	0.60	6.29	4.16	254,776.270	644.74	0.13	0.96	655.89	<0.012	6.970	7.150	2.9200	0.166	10.690	<0.001	0.830	<0.001	1.140	0.095
20ALS4E	Chalcopyrite	305,909	3.60	0.013	1.87	0.62	7.10	4.48	258,245.770	1049.00	1.21	0.80	646.76	0.036	15.390	9.280	2.7600	0.410	17.650	<0.001	0.810	0.005	11.630	0.259
20ALS3S1	Chalcopyrite	410,396	4.19	0.037	2.07	0.10	0.05	14.17	330,386.130	520.62	0.89	2.10	280.24	0.718	21.020	8.930	23.2000	0.310	12.810	<0.001	0.530	0.004	1.118	0.230
20ALS3S1	Chalcopyrite	393,338	3.19	0.031	0.71	0.68	0.10	14.78	311,331.380	649.03	<0.17	2.19	259.54	0.627	21.220	9.930	23.2200	0.340	15.260	<0.001	1.620	<0.001	1.043	0.260
20ALS3S1	Chalcopyrite	418,722	5.01	<0.008	2.28	1.08	0.10	13.07	328,668.000	503.12	0.23	2.95	267.21	0.857	19.350	10.380	22.9800	0.510	18.920	<0.001	0.660	<0.001	0.428	0.120
20ALS3S1	Chalcopyrite	407,357	36.37	2.850	18.36	9.71	0.13	16.07	315,585.440	1062.20	0.91	1.31	278.47	0.495	22.340	15.930	20.0800	0.318	13.750	<0.001	1.000	0.012	1.530	0.300
20ALS3S1	Chalcopyrite	383,288	3.15	<0.006	1.09	0.71	0.07	16.53	319,104.090	634.99	0.89	2.29	255.81	0.681	19.940	11.300	18.6900	0.410	19.210	<0.001	0.900	<0.002	0.742	0.210
20ALS3S1	Chalcopyrite	381,877	3.47	0.036	1.64	0.58	0.05	12.17	325,434.590	551.32	<0.13	1.93	264.56	0.834	31.000	11.670	18.7500	0.380	15.240	<0.001	0.230	0.007	1.900	0.290
20ALS4F	Chalcopyrite	412,434	3.59	<0.008	1.52	0.76	7.20	16.56	322,072.470	674.34	<0.13	1.66	425.09	0.508	15.800	8.570	3.2000	0.280	13.360	<0.001	1.250	<0.001	1.137	0.410
20ALS4F	Chalcopyrite	375,728	3.42	<0.006	1.51	0.65	7.18	17.65	305,306.130	512.15	<0.10	2.23	367.45	0.740	14.370	6.030	3.0300	0.312	13.700	0.004	1.360	0.004	0.560	0.260
20ALS4F	Chalcopyrite	422,622	2.40	0.066	2.23	0.19	6.95	17.95	321,485.440	539.14	0.35	2.73	398.63	0.643	12.470	7.220	3.7600	0.450	19.830	<0.001	1.060	<0.001	0.948	0.680
20ALS4F	Chalcopyrite	423,474	3.25	<0.007	1.49	0.52	11.66	19.62	335,244.590	575.54	1.59	1.70	408.71	0.780	12.820	7.540	3.8700	0.510	18.560	0.004	1.010	0.003	1.327	1.340
20ALS4F	Chalcopyrite	429,318	3.86	0.012	2.51	0.36	6.65	19.36	312,942.530	538.85	0.94	1.78	433.69	0.692	12.050	7.250	3.8900	0.500	18.800	<0.001	1.190	0.005	0.769	2.720
20ALS4F	Pyrite	373,918	2.40	0.012	2.44	0.66	6.97	17.29	8.110	439.64	0.71	2.57	352.49	0.687	14.250	5.260	3.0100	0.275	10.740	<0.001	0.640	0.005	0.752	0.200
20ALS4F	Pyrite	598,686	4.92	0.027	<0.10	0.52	464.26	4.42	3.770	<0.09	0.84	51.42	617.47	1.293	0.044	<0.0065	0.0007	2.220	17.120	<0.001	0.290	<0.001	1.680	1.440
20ALS4F	Pyrite	627,569	6.31	0.041	<0.11	0.59	330.71	2.81	49.510	56.13	0.51	151.43	723.19	2.200	0.509	0.530	0.0246	1.700	36.380	0.006	0.730	<0.001	1.234	0.670
20ALS4F	Pyrite	546,416	5.19	0.005	<0.10	0.47	188.01	1.43	1.515	0.66	0.71	239.18	544.39	1.473	0.044	<0.008	<0.0005	1.020	25.590	0.004	0.250	<0.001	0.658	0.420
20ALS4F	Pyrite	560,038	5.55	<0.003	<0.09	0.43	17.15	1.63	0.357	<0.10	0.81	1.66	264.71	1.730	0.002	<0.0056	<0.0001	0.073	1.199	<0.001	<0.03	0.002	0.118	0.050
20ALS3S1	Pyrite	655,913	5.97	<0.004	<0.11	0.44	4866.86	4.91	0.446	0.62	1.25	257.17	156.21	1.520	0.024	0.014	<0.0007	<0.002	<0.016	<0.001	0.074	0.003	<0.001	<0.001
20ALS3S1	Pyrite	608,411	5.62	0.016	<0.108	0.57	123.61	20.47	0.324	<0.10	1.11	104.22	159.12	1.363	<0.003	<0.014	<0.0001	0.005	0.175	<0.001	0.530	<0.001	<0.001	<0.001
20ALS3S1	Pyrite	568,996	5.56	0.039	<0.11	0.62	3302.34	2.41	0.625	<0.10	0.86	0.60	79.76	1.440	<0.005	<0.011	0.0037	0.088	1.800	<0.001	0.080	<0.001	0.076	1.980
20ALS4E	Pyrite	174,297	2.35	0.021	1.33	0.44	645.50	216.37	0.273	<0.12	0.36	0.73	208.74	0.050	0.036	0.074	0.0016	0.015	0.486	<0.001	<0.05	<0.001	0.145	0.003

Table A1. *Cont.*

Sample	Mineral	S	Ti	V	Cr	Mn	Co	Ni	Cu	Zn	Ge	As	Se	Mo	Ag	Cd	In	Sb	Te	Au	Hg	Tl	Pb	Bi
																							(ppm)	
The Lindøya basalt-hosted VMS deposit																								
20LIND4B	Pyrite	419,160	5.95	0.203	<0.08	3.52	1.57	20.11	1.750	<0.07	0.46	729.49	<0.37	<0.006	<0.001	<0.003	0.0035	0.029	<0.008	<0.001	0.130	0.023	0.109	<0.001
20LIND4B	Pyrite	402,121	6.34	1.630	<0.09	21.66	0.14	17.28	14.660	1.69	0.73	1907.67	<0.40	0.015	0.018	0.042	0.0026	0.310	<0.010	0.002	0.230	0.267	0.450	0.001
20LIND4B	Pyrite	386,882	6.92	1.320	<0.08	10.40	0.03	3.83	0.514	0.12	0.73	655.35	4.66	0.058	0.005	<0.005	<0.0003	0.030	<0.007	<0.001	0.200	0.015	0.071	<0.001
20LIND4B	Pyrite	374,520	104.49	23.770	4.73	169.44	8.48	32.73	238.420	25.22	1.21	783.17	<0.48	12.730	1.670	0.530	0.0105	50.460	0.249	0.016	12.960	3.310	120.160	0.151
20LIND4B	Pyrite	393,781	91.88	42.550	6.64	139.63	8.51	36.14	241.460	28.71	1.00	786.08	<0.51	12.940	1.620	0.240	0.0108	51.420	0.264	0.019	13.630	3.310	125.200	0.157
20LIND4B	Pyrite	425,634	200.89	47.960	10.31	150.51	9.48	34.98	252.110	28.03	0.83	891.97	<0.65	12.950	1.810	0.520	0.0097	56.900	<0.017	0.018	14.710	3.750	135.020	0.169
20LIND4B	Pyrite	431,081	13.40	4.000	<0.095	19.42	7.03	15.09	25.240	11,692.87	1.13	854.40	<0.45	4.830	0.198	24.890	0.3410	1.160	0.015	<0.001	6.710	0.480	2.670	0.002
20LIND4B	Pyrite	450,316	8.01	1.650	0.68	12.63	10.71	18.65	49.680	3082.57	0.84	839.24	0.89	11.720	0.111	9.000	0.1350	2.630	<0.010	0.002	2.400	0.232	5.940	0.006
20LIND4B	Pyrite	418,035	5.75	0.333	<0.08	4.34	4.37	15.18	8.230	542.40	0.74	563.45	<0.39	0.189	0.028	2.150	0.0190	1.020	<0.009	<0.001	0.670	0.073	2.810	<0.001
20LIND4B	Pyrite	396,140	83.12	27.310	6.90	124.16	10.43	26.44	220.970	23.85	0.59	799.63	<0.51	15.420	1.540	0.390	0.0016	45.940	0.076	0.019	11.950	2.740	126.900	0.181
20LIND4B	Pyrite	379,951	79.59	22.540	8.04	82.45	10.10	27.48	200.210	22.48	0.90	719.34	<0.50	14.280	1.280	0.370	0.0037	40.510	0.274	0.022	9.950	2.330	104.110	0.180
20LIND4B	Pyrite	418,002	60.85	30.760	8.18	124.84	10.76	28.21	257.940	24.53	1.18	840.28	<0.54	15.730	1.640	0.470	0.0013	47.380	0.253	0.017	12.740	2.660	131.160	0.220
20LIND4B	Pyrite	429,217	5.43	0.004	0.24	0.49	0.13	39.95	5.300	1.97	0.94	450.16	<0.38	<0.007	0.018	0.012	<0.0004	0.250	0.048	<0.001	0.057	0.147	0.540	<0.001
20LIND4B	Pyrite	410,436	6.10	0.024	<0.09	0.47	0.05	1.66	7.850	<0.07	0.95	1173.57	<0.43	<0.006	0.020	0.032	0.0024	0.310	0.041	<0.001	0.150	0.090	0.446	<0.001
20LIND4B	Pyrite	395,000	8.55	0.380	0.41	0.69	2.23	14.25	1.200	<0.07	0.79	646.76	1.63	0.081	<0.001	0.054	<0.0004	0.055	0.099	<0.001	0.340	0.072	0.156	0.001
20LIND4B	Pyrite	367,116	94.72	26.750	5.51	140.70	9.47	39.07	214.420	28.09	6.06	771.31	<0.48	12.590	1.460	0.270	0.0122	42.210	0.201	0.030	11.580	3.170	104.790	0.113
20LIND4B	Pyrite	378,458	194.41	34.070	5.37	148.29	7.03	38.02	230.050	23.68	1.02	713.20	1.48	9.400	1.610	0.420	0.0076	45.330	0.137	0.038	12.380	3.100	121.040	0.158
20LIND4B	Pyrite	417,445	128.75	23.630	4.40	170.52	8.30	38.88	245.300	27.98	0.60	776.90	2.81	7.650	1.890	0.340	0.0130	51.670	0.205	0.028	14.510	3.470	131.350	0.167
The Litlabø sediment-hosted VMS deposit																								
19LIT2	Pyrite-1	602,687	7.90	1.340	<0.10	16.87	1.85	13.88	3.340	15.43	1.74	643.88	3.53	2.190	0.802	0.160	<0.0006	5.060	0.110	0.057	0.320	0.126	18.530	0.130
19LIT2	Pyrite-1	537,316	10.68	11.850	8.63	29.83	1.13	7.41	1.290	2.12	0.91	423.21	6.22	2.660	0.090	<0.014	<0.0009	0.930	0.093	<0.001	0.420	0.101	3.530	0.006
19LIT2	Pyrite-1	546,070	78.33	13.150	3.91	26.78	2.16	13.34	1.880	3.87	1.06	739.96	6.28	1.630	0.638	<0.011	0.0106	3.540	0.057	<0.001	0.220	0.970	12.440	0.084
19LIT2	Pyrite-1	542,973	77.94	43.430	4.96	21.50	9.13	88.87	18.120	46.57	1.12	1104.23	<0.68	30.560	1.290	0.570	0.0304	18.670	0.262	0.022	0.550	0.940	64.280	0.280
19LIT2	Pyrite-1	460,554	11.18	1.520	0.59	4.75	7.04	64.95	8.090	36.60	0.84	938.06	5.06	5.830	0.622	0.340	0.0040	12.160	0.156	0.038	0.420	0.460	37.740	0.180
19LIT2	Pyrite-2	564,288	66.82	9.190	1.11	13.41	8.21	23.36	6.000	29.39	1.43	718.63	<0.59	17.550	0.553	0.043	<0.0014	9.730	0.202	<0.00	0.510	0.870	29.340	0.140
19LIT2	Pyrite-2	563,554	14.72	52.330	33.38	82.09	6.12	8.95	2.050	8.58	1.38	626.72	5.04	1.300	0.260	0.080	<0.0012	0.690	0.116	0.004	0.880	0.343	5.730	0.017
19LIT2	Pyrite-2	530,704	6.78	1.630	0.39	14.56	8.69	21.37	1.470	0.31	1.62	558.28	4.99	13.400	0.080	<0.011	0.0020	1.610	<0.015	0.002	0.290	0.121	4.830	0.026
19LIT2	Pyrite-2	555,489	29.93	8.030	2.01	6.82	3.23	21.04	4.700	13.38	1.11	902.36	7.89	5.970	0.980	0.096	0.0045	7.520	0.098	0.049	0.610	0.291	23.070	0.150
19LIT2	Pyrite-2	610,325	13.67	6.940	2.55	14.99	2.50	16.94	10.790	11.20	1.57	919.01	1.96	6.740	0.629	0.150	0.0141	3.380	0.026	0.038	0.300	0.560	18.110	0.058
19LIT2	Pyrite-2	607,653	7.15	1.250	<0.10	27.82	2.08	10.07	1.380	1.09	1.15	553.04	6.25	2.380	0.164	0.230	<0.0015	1.580	0.175	0.012	<0.040	0.113	4.760	0.040

References

1. Piercey, S.J. An overview of petrochemistry in the regional exploration for volcanogenic massive sulphide (VMS) deposits. *Geochem. Explor. Environ. Anal.* **2010**, *10*, 119–136. [CrossRef]
2. Torró, L.; Benites, D.; Vallance, J.; Laurent, O.; Ortiz-Benavente, B.A.; Michou, C.C.; Proenza, J.A.; Fontboté, L. Trace element geochemistry of sphalerite and chalcopyrite in arc-hosted VMS deposits. *J. Geochem. Explor.* **2022**, *232*, 106882. [CrossRef]
3. Yesares, L.; Pina, R.; Gonzalez-Jimenez, J.M.; Saez, R.; de Almodovar, G.R.; Fanlo, I.; Pons, J.M.; Vega, R. Distribution of critical metals in evolving pyrite from massive sulfide ores of the Iberian Pyrite Belt. *Ore Geol. Rev.* **2023**, *153*, 105275. [CrossRef]
4. Barrie, C.T.; Cathles, L.M.; Erendi, A.; Schwaiger, H.; Murray, C.; Hannington, M.D. Heat and fluid flow in volcanic-associated massive sulfide-forming hydrothermal systems. *Rev. Econ. Geol.* **1999**, *8*, 201–219.
5. Galley, A.G.; Hannington, M.D.; Jonasson, I.R. Volcanogenic massive sulphide deposits. In *Mineral Deposits of Canada: A Synthesis of Major Deposit-Types, District Metallogeny, the Evolution of Geological Provinces, and Exploration Methods*; Goodfellow, W.D., Ed.; Geological Association of Canada, Mineral Deposits Division: St. John's, NL, Canada, 2007; Volume 5, pp. 141–161.
6. Piercey, S.J. The setting, style, and role of magmatism in the formation of volcanogenic massive sulfide deposits. *Miner. Depos.* **2011**, *46*, 449–471. [CrossRef]
7. Ross, P.S.; Mercier-Langevin, P. Igneous Rock Associations 14. The volcanic setting of VMS and SMS deposits: A review. *Geosci. Can.* **2014**, *41*, 365–377. [CrossRef]
8. Hannington, M.D. Volcanogenic massive sulfide deposits. *Treatise Geochem.* **2014**, *13*, 463–488.
9. Patten, C.G.; Coltat, R.; Junge, M.; Peillod, A.; Ulrich, M.; Manatschal, G.; Kolb, J. Ultramafic-hosted volcanogenic massive sulfide deposits: An overlooked sub-class of VMS deposit forming in complex tectonic environments. *Earth Sci. Rev.* **2022**, *224*, 103891. [CrossRef]
10. Grenne, T.; Ihlen, P.M.; Vokes, F.M. Scandinavian Caledonide metallogeny in a plate tectonic perspective. *Miner. Depos.* **1999**, *34*, 422–471. [CrossRef]
11. Corfu, F.; Andersen, T.B.; Gasser, D. The Scandinavian Caledonides: Main features, conceptual advances and critical questions. *Geol. Soc. Lond. Spec. Publ.* **2014**, *390*, 9–43. [CrossRef]
12. Dunning, G.R.; Pedersen, R.B. U/Pb ages of ophiolites and arc-related plutons of the Norwegian Caledonides: Implications for the development of Iapetus. *Contrib. Miner. Petrol.* **1988**, *98*, 13–23. [CrossRef]
13. Pedersen, R.B.; Furnes, H. Geology, magmatic affinity and geotectonic environment of some Caledonian ophiolites in Norway. *J. Geodyn.* **1991**, *13*, 183–203. [CrossRef]
14. Roberts, D. The Scandinavian Caledonides: Event chronology, palaeogeographic settings and likely modern analogues. *Tectonophysics* **2003**, *365*, 283–299. [CrossRef]
15. Wulff, P.W. *En Befaring af Cirka 100 Mineraliseringer i Sunnhordland, SV-Norge*; NGU-rapport 96.139; Norges Geologiske Undersøkelse: Trondheim, Norway, 1996.
16. Forsberg, F.R. Geochemical Characteristics of the Gold-Bearing Quartz Veins in the Lykling Area, Bømlo, SW Norway. Master's Thesis, University of Bergen, Bergen, Norway, September 2021.
17. Paulsson, O.; Andréasson, P.G. Attempted break-up of Rodinia at 850 Ma: Geochronological evidence from the Seve–Kalak Superterrane, Scandinavian Caledonides. *J. Geol. Soc.* **2002**, *159*, 751–761. [CrossRef]
18. Gee, D.G. Caledonides of the North Atlantic Region and Occurrence of Ophiolites. *Acta Geol. Sin. (Engl. Ed.)* **2015**, *89*, 13–14. [CrossRef]
19. Hacker, B.R.; Gans, P.B. Continental collisions and the creation of ultrahigh-pressure terranes: Petrology and thermochronology of nappes in the central Scandinavian Caledonides. *Geol. Soc. Am. Bull.* **2005**, *117*, 117–134. [CrossRef]
20. Slagstad, T.; Kirkland, C.L. Timing of collision initiation and location of the Scandian orogenic suture in the Scandinavian Caledonides. *Terra Nova* **2018**, *30*, 179–188. [CrossRef]
21. Fossen, H.; Hurich, C.A. The Hardangerfjord Shear Zone in SW Norway and the North Sea: A large-scale low-angle shear zone in the Caledonian crust. *J. Geol. Soc.* **2005**, *162*, 675–687. [CrossRef]
22. Pedersen, R.B.; Furnes, H.; Dunning, G. Some Norwegian ophiolite complexes reconsidered. *Nor. Geol. Unders. Spec. Publ.* **1988**, *3*, 80–85.
23. Furnes, H.; Pedersen, R.B.; Hertogen, J.; Albrektsen, B.A. Magma development of the Leka ophiolite complex, central Norwegian Caledonides. *Lithos* **1991**, *27*, 259–277. [CrossRef]
24. Pedersen, R.B.; Furnes, H.; Dunning, G. AU/Pb age for the Sulitjelma Gabbro, north Norway: Further evidence for the development of a Caledonian marginal basin in Ashgill–Llandovery time. *Geol. Mag.* **1991**, *128*, 141–153. [CrossRef]
25. Slagstad, T.; Pin, C.; Roberts, D.; Kirkland, C.L.; Grenne, T.; Dunning, G.; Sauer, S.; Andersen, T. Tectonomagmatic evolution of the Early Ordovician suprasubduction-zone ophiolites of the Trondheim Region, Mid-Norwegian Caledonides. *Geol. Soc. Lond. Spec. Publ.* **2014**, *390*, 541–561. [CrossRef]
26. Norwegian Geological Survey. Berggrunn—Nasjonal Berggrunnsdatabase. Available online: https://geo.ngu.no/kart/berggrunn_mobil/ (accessed on 25 March 2024).
27. Brekke, H.; Furnes, H.; Nordås, J.; Hertogen, J. Lower Palaeozoic convergent plate margin volcanism on Bømlo, SW Norway, and its bearing on the tectonic environments of the Norwegian Caledonides. *J. Geol. Soc.* **1984**, *141*, 1015–1032. [CrossRef]

28. Nordås, J.; Amaliksen, K.; Brekke, H.; Suthern, R.; Furnes, H.; Sturt, B.; Robins, B.; Gee, D. Lithostratigraphy and petrochemistry of Caledonian rocks on Bømlo, SW Norway. In *The Caledonide Orogen—Scandinavia and Related Areas*; Gee, D.G., Sturt, B.A., Eds.; John Wiley & Sons Ltd.: New York, USA, 1985; pp. 679–692.

29. Pedersen, R.B.; Dunning, G.R. Evolution of arc crust and relations between contrasting sources: U-Pb (age), Nd and Sr isotope systematics of the ophiolitic terrain of SW Norway. *Contrib. Miner. Petrol.* **1997**, *128*, 1–15. [CrossRef]

30. Andersen, T.B.; Jansen, Ø.J. The Sunnhordland Batholith, W. Norway: Regional setting and internal structure, with emphasis on the granitoid plutons. *Nor. Geol. Tidsskr.* **1987**, *67*, 159–183.

31. Scheiber, T.; Viola, G.; Wilkinson, C.M.; Ganerød, M.; Skår, Ø.; Gasser, D. Direct 40Ar/39Ar dating of Late Ordovician and Silurian brittle faulting in the southwestern Norwegian Caledonides. *Terra Nova* **2016**, *28*, 374–382. [CrossRef]

32. Amaliksen, K. The Geology of the Lvkling Ophiolitic Complex, Bømlo, SW Norway. Unpubl. PhD Thesis, Bergen University, Bergen, Norway, 1983.

33. Fjellet, T. Geochemical Characteristics of Volcanogenic Massive Sulfide Mineralizations on Bømlo and Stord Islands, Sunnhordaland, SW Norway. Master's Thesis, University of Bergen, Bergen, Norway, August 2021.

34. Van Achterberg, E.; Ryan, C.; Jackson, S.E.; Griffin, W.L. Data reduction software for LA-ICP-MS. In *Laser Ablation-ICP-Mass Spectrometry in the Earth Sciences: Principles and Applications*; Mineralogical Association of Canada: Ottawa, ON, Canada, 2001; pp. 239–243.

35. Spangenberg, J.E.; Saintilan, N.J.; Palinkaš, S.S. Safe, accurate, and precise sulfur isotope analyses of arsenides, sulfarsenides, and arsenic and mercury sulfides by conversion to barium sulfate before EA/IRMS. *Anal. Bioanal. Chem.* **2022**, *414*, 2163–2179. [CrossRef] [PubMed]

36. Warr, L.N. IMA–CNMNC approved mineral symbols. *Miner. Mag.* **2021**, *85*, 291–320. [CrossRef]

37. Norwegian Geological Survey Mineral Resource Database. Available online: https://www.ngu.no/en/geologiske-kart/datasett (accessed on 25 March 2024).

38. Pirajno, F.; Uysal, I.; Naumov, E.A. Oceanic lithosphere and ophiolites: Birth, life and final resting place of related ore deposits. *Gondwana Res.* **2020**, *88*, 333–352. [CrossRef]

39. Foose, M.P. *The Setting of a Magmatic Sulfide Occurrence in a Dismembered Ophiolite, Southwest Oregon*; Distribution Branch; USA Geological Survey: Reston, VA, USA, 1985; p. 1626.

40. Bacuta, G.C.; Kay, R.W.; Gibbs, A.K.; Lipin, B.R. Platinum-group element abundance and distribution in chromite deposits of the Acoje Block. *Zambales ophiolite Complex, Philippines. J. Geochem. Explor.* **1990**, *37*, 113–145. [CrossRef]

41. Lorand, J.P.; Juteau, T. The Haymiliyah sulphide ores (Haylayn Massif, Oman Ophiolite): In-situ segregation of PGE-poor magmatic sulphides in a fossil oceanic magma chamber. *Mar. Geophys. Res.* **2000**, *21*, 327–350. [CrossRef]

42. Baumgartner, R.J.; Zaccarini, F.; Garuti, G.; Thalhammer, O.A.R. Mineralogical and geochemical investigation of layered chromitites from the Bracco–Gabbro complex, Ligurian ophiolite, Italy. *Contrib. Miner. Pet.* **2013**, *165*, 477–493. [CrossRef]

43. Cook, N.J.; Ciobanu, C.L.; George, L.L.; Crowe, B.; Wade, B.P. Trace element distributions in sulphides: Progress, problems and perspectives. *Acta Geol. Sin. (Engl. Ed.)* **2014**, *88*, 1444–1446. [CrossRef]

44. Wohlgemuth-Ueberwasser, C.C.; Viljoen, F.; Petersen, S.; Vorster, C. Distribution and solubility limits of trace elements in hydrothermal black smoker sulfides: An in-situ LA-ICP-MS study. *Geochim. Cosmochim. Acta* **2015**, *159*, 16–41. [CrossRef]

45. Duran, C.J.; Dubé-Loubert, H.; Pagé, P.; Barnes, S.-J.; Roy, M.; Savard, D.; Cave, B.J.; Arguin, J.P.; Mansur, E.T. Applications of trace element chemistry of pyrite and chalcopyrite in glacial sediments to mineral exploration targeting: Example from the Churchill Province, northern Quebec, Canada. *J. Geochem. Explor.* **2019**, *196*, 105–130. [CrossRef]

46. Raič, S.; Molnár, F.; Cook, N.; OBrien, H.; Lahaye, Y. Application of lithogeochemical and pyrite trace element data for the determination of vectors to ore in the Raja Au-Co prospect, Northern Finland. *Solid Earth Discuss.* **2021**, *13*, 1–49. [CrossRef]

47. Reich, M.; Simon, A.C.; Deditius, A.; Barra, F.; Chryssoulis, S.; Lagas, G.; Tardani, D.; Knipping, J.; Bilenker, L.; Sánchez-Alfaro, P.; et al. Trace element signature of pyrite from the Los Colorados iron oxide-apatite (IOA) deposit, Chile: A missing link between Andean IOA and iron oxide copper-gold systems? *Econ. Geol.* **2016**, *111*, 743–761. [CrossRef]

48. Sykora, S.; Cooke, D.R.; Meffre, S.; Stephanov, A.S.; Gardner, K.; Scott, R.; Selley, D.; Harris, A.C. Evolution of pyrite trace element compositions from porphyry-style and epithermal conditions at the Lihir gold deposit: Implications for ore genesis and mineral processing. *Econ. Geol.* **2018**, *113*, 193–208. [CrossRef]

49. Strmić Palinkaš, S.; Hofstra, A.H.; Percival, T.J.; Šoštarić, S.B.; Palinkaš, L.; Bermanec, V.; Pecskay, Z.; Boev, B. Comparison of the Allchar Au-As-Sb-Tl Deposit, Republic of Macedonia, with Carlin-Type Gold Deposits. In *Diversity in Carlin-Style Gold Deposits*; Muntean, J.L., Ed.; Society of Economic Geologists: Littleton, CO, USA, 2018; Volume 20.

50. Steadman, J.A.; Large, R.R.; Olin, P.H.; Danyushevsky, L.V.; Meffre, S.; Huston, D.; Fabris, A.; Lisitsin, V.; Wells, T. Pyrite trace element behavior in magmatic-hydrothermal environments: An LA-ICPMS imaging study. *Ore Geol. Rev.* **2021**, *128*, 103878. [CrossRef]

51. Genna, D.; Gaboury, D. Deciphering the hydrothermal evolution of a VMS system by LA-ICP-MS using trace elements in pyrite: An example from the Bracemac-McLeod deposits, Abitibi, Canada, and implications for exploration. *Econ. Geol.* **2015**, *110*, 2087–2108. [CrossRef]

52. Belousov, I.; Large, R.R.; Meffre, S.; Danyushevsky, L.V.; Steadman, J.; Beardsmore, T. Pyrite compositions from VHMS and orogenic Au deposits in the Yilgarn Craton, Western Australia: Implications for gold and copper exploration. *Ore Geol. Rev.* **2016**, *79*, 474–499. [CrossRef]

53. Dehnavi, A.S.; McFarlane, C.R.; Lentz, D.R.; Walker, J.A. Assessment of pyrite composition by LA-ICP-MS techniques from massive sulfide deposits of the Bathurst Mining Camp, Canada: From textural and chemical evolution to its application as a vectoring tool for the exploration of VMS deposits. *Ore Geol. Rev.* **2018**, *92*, 656–671. [CrossRef]

54. Maslennikov, V.V.; Maslennikova, S.P.; Large, R.R.; Danyushevsky, L.V. Study of trace element zonation in vent chimneys from the Silurian Yaman-Kasy volcanic-hosted massive sulfide deposit (Southern Urals, Russia) using laser ablation-inductively coupled plasma mass spectrometry (LA-ICPMS). *Econ. Geol.* **2009**, *104*, 1111–1141. [CrossRef]

55. Layton-Matthews, D.; Leybourne, M.I.; Peter, J.M.; Scott, S.D.; Cousens, B.; Eglington, B.M. Multiple sources of selenium in ancient seafloor hydrothermal systems: Compositional and Se, S, and Pb isotopic evidence from volcanic-hosted and volcanic-sediment-hosted massive sulfide deposits of the Finlayson Lake District, Yukon, Canada. *Geochim. Cosmochim. Acta* **2013**, *117*, 313–331. [CrossRef]

56. Martin, A.J.; McDonald, I.; MacLeod, C.J.; Prichard, H.M.; McFall, K. Extreme enrichment of selenium in the Apliki Cyprus-type VMS deposit, Troodos, Cyprus. *Miner. Mag.* **2018**, *82*, 697–724. [CrossRef]

57. Martin, A.J.; McDonald, I.; Jamieson, J.W.; Jenkin, G.R.T.; McFall, K.A.; Piercey, G.; MacLeod, C.J.; Layne, G.D. Mineral-scale variation in the trace metal and sulfur isotope composition of pyrite: Implications for metal and sulfur sources in mafic VMS deposits. *Miner. Depos.* **2021**, *57*, 911–933. [CrossRef]

58. Duran, C.J.; Barnes, S.-J.; Corkery, J.T. Chalcophile and platinum-group element distribution in pyrites from the sulfide-rich pods of the Lac des Iles Pd deposits, Western Ontario, Canada: Implications for post-cumulus re-equilibration of the ore and the use of pyrite compositions in exploration. *J. Geochem. Explor.* **2015**, *158*, 223–242. [CrossRef]

59. Huston, D.L.; Sie, S.H.; Suter, G.F.; Cooke, D.R.; Both, R.A. Trace elements in sulfide minerals from eastern Australian volcanic-hosted massive sulfide deposits; Part I, Proton microprobe analyses of pyrite, chalcopyrite, and sphalerite, and Part II, Selenium levels in pyrite; comparison with delta 34 S values and implications for the source of sulfur in volcanogenic hydrothermal systems. *Econ. Geol.* **1995**, *90*, 1167–1196.

60. George, L.L.; Cook, N.J.; Ciobanu, C.L. Partitioning of trace elements in co-crystallized sphalerite–galena–chalcopyrite hydrothermal ores. *Ore Geol. Rev.* **2016**, *77*, 97–116. [CrossRef]

61. George, L.L.; Cook, N.J.; Crowe, B.B.; Ciobanu, C.L. Trace elements in hydrothermal chalcopyrite. *Miner. Mag.* **2018**, *82*, 59–88. [CrossRef]

62. Sahlström, F.; Palinkaš, S.S.; Dundas, S.H.; Sendula, E.; Cheng, Y.; Wold, M.; Pedersen, R.B. Mineralogical distribution and genetic aspects of cobalt at the active Fåvne and Loki's Castle seafloor massive sulfide deposits, Arctic Mid-Ocean Ridges. *Ore Geol. Rev.* **2023**, *153*, 105261. [CrossRef]

63. Herzig, P.M.; Hannington, M.D.; Arribas, A., Jr. Sulfur isotopic composition of hydrothermal precipitates from the Lau back-arc: Implications for magmatic contributions to seafloor hydrothermal systems. *Miner. Depos.* **1998**, *33*, 226–237. [CrossRef]

64. Hannington, M.D.; de Ronde, C.E.J.; Petersen, S. Sea-floor tectonics and submarine hydrothermal systems. In *One Hundreth Anniversary Volume 1905—2005*; Hedenquist, J.W., Thompson, J.F.H., Goldfarb, R.J., Richards, J.P., Eds.; Society of Economic Geologists: Littleton, CO, USA, 2005; pp. 111–141.

65. Garuti, G.; Alfonso, P.; Proenza, J.A.; Zaccarini, F. Sulfur-isotope variations in sulfide minerals from massive sulfide deposits of the northern Apennine ophiolites: Inorganic and biogenic constraints. *Ofioliti* **2009**, *34*, 43–62.

66. Grenne, T.; Slack, J.F. Mineralogy and geochemistry of silicate, sulfide, and oxide iron formations in Norway: Evidence for fluctuating redox states of early Paleozoic marine basins. *Miner. Depos.* **2019**, *54*, 829–848. [CrossRef]

67. Ohmoto, H. Formation of volcanogenic massive sulfide deposits: The Kuroko perspective. *Ore Geol. Rev.* **1996**, *10*, 135–177. [CrossRef]

68. Velasco, F.; Sánchez-España, J.; Boyce, A.J.; Fallick, A.E.; Sáez, R.; Almodóvar, G.R. A new sulphur isotopic study of some Iberian Pyrite Belt deposits: Evidence of a textural control on sulphur isotope composition. *Miner. Depos.* **1998**, *34*, 4–18. [CrossRef]